Formation of hydrothermal REE-phosphate deposits

STEFAN S. ANDERSSON

ACADEMIC DISSERTATION
To be presented, with the permission of the Faculty of Science of the University of Helsinki, for public examination in auditorium D101, Physicum, Kumpula Campus, on May 29 2019, at 12 noon.

DEPARTMENT OF GEOSCIENCES AND GEOGRAPHY A76 / HELSINKI 2019

Cover photo: Highly birefringent and fractured xenotime in Djupedal (© Stefan S. Andersson, field of view is 5 mm)

Author´s address: Stefan S. Andersson
Department of Geosciences and Geography
P.O. Box 64
00014 University of Helsinki, Finland
stefan.andersson@helsinki.fi (steffe@gmail.com)

Supervised by: Professor Thomas Wagner
Institute of Applied Mineralogy and Economic Geology
RWTH Aachen University
&
Department of Geosciences and Geography
University of Helsinki

Dr. Erik Jonsson
Department of Mineral Resources
Geological Survey of Sweden
&
Department of Earth Sciences
Uppsala University

Reviewed by: Professor Martin Smith
School of Environment and Technology
University of Brighton

Priv.-Doz. Dr. Michael Marks
Department of Geosciences
University of Tübingen

Opponent: Professor emeritus Ulf Hålenius
Swedish Museum of Natural History

ISSN-L 1798-7911
ISSN 1798-7911 (print)
ISBN 978-951-51-4915-2 (paperback)
ISBN 978-951-51-4916-9 (PDF)

http://ethesis.helsinki.fi

Unigrafia
Helsinki 2019

The Faculty of Science uses the Urkund system (plagiarism recognition) to examine all doctoral dissertations.

Andersson S.S., 2019. *The formation of hydrothermal REE-phosphate deposits*. Unigrafia. Helsinki. 53 pages, 4 tables and 7 figures.

Abstract

Rare earth elements (REE) are important metals used in green and low-carbon energy and information technologies and are widely used for geological petrogenetic studies. It is becoming increasingly evident that the REE can be mobile in certain hydrothermal fluids and even form hydrothermal REE deposits. This study focuses on the formation of hydrothermal REE deposits rich in the REE-phosphates (monazite [(LREE,Y)PO_4] and xenotime [(Y,HREE)PO_4]). The main objective of the study was to characterise the Olserum-Djupedal REE-phosphate mineralisation in SE Sweden. Based on this, the study evaluates different sources of REE and P in hydrothermal deposits and assesses how REE and P are transported in hydrothermal fluids. To characterise the Olserum-Djupedal REE mineralisation, this study combines fieldwork, petrographical and textural analysis, major and trace element mineral chemistry of REE-bearing minerals and the main gangue phases, stable Cl isotopic and halogen analysis of fluorapatite, and fluid inclusion microthermometry and LA-ICP-MS analysis.

The primary Olserum-Djupedal REE mineralisation comprises co-existing monazite-(Ce), xenotime-(Y) and fluorapatite. These occur mainly within veins dominated by biotite, magnetite, gedrite and quartz forming within metasedimentary rocks in or close to the contact aureole of a peraluminous alkali feldspar granite. The veins are also hosted by the granite within the outermost part of this granite. Primary REE-minerals formed by granitic-derived NaCl-$FeCl_2$-KCl-$CaCl_2$-HF-H_2O fluids at high temperatures of ~600 °C at c. 1.8 Ga. Subsequently, the ore assemblages were variably modified during cooling by $CaCl_2$-NaCl to NaCl-$CaCl_2$ brines, and partly, CO_2-rich fluids down to temperatures of ~300 °C and to at least 1.75 Ga.

Hydrothermal REE deposits rich in REE-phosphates are commonly associated with alkaline magmatism, particularly in silicate-carbonatitic systems. This is because REE and P both exhibit strong chemical affinities with carbonatitic systems and the potential for mobilisation of REE and P are high. This study shows that REE deposits can also form by hydrothermal activity related to subalkaline magmatic rocks. Peraluminous granites exhibit the greatest potential to exsolve fluids carrying REE and P, which can lead to the formation of hydrothermal REE deposits rich in REE-phosphates.

The general understanding on how hydrothermal REE-phosphate deposits form is that REE and P are transported in separate fluids and that the REE-phosphates form when these two fluids mix, or the REE-phosphates form when REE-bearing fluids interact with P-rich rocks. The lack of rocks pre-enriched in P in the Olserum-Djupedal district and the co-crystallisation of fluorapatite, monazite-(Ce) and xenotime-(Y), however, suggest that such scenarios not necessarily account for all occurrences of hydrothermal REE-phosphate deposits. As an alternative, REE and P can have been transported by the same fluid. This study dem-

onstrates that the most probable conditions for co-transport of REE and P are at temperatures exceeding 400 °C and with increasing salinity of the fluids, conditions that agree well with that of the Olserum-Djupedal system. The most effective co-transport of REE and P would occur at acidic conditions by REE-Cl, REE-F or REE-SO_4 complexes. Yet, co-transport of REE and P may also be feasible at neutral to alkaline conditions by REE-OH complexes. In low-temperature hydrothermal systems, the interaction of REE-bearing fluids with P-rich rocks or fluids is probably the most efficient mechanism for precipitating REE-phosphates. In high-temperature magmatic-hydrothermal systems, REE and P probably share a common origin and were transported by the same fluid. In such systems, pH changes, cooling and the destabilisation of the chief REE transporting complexes jointly contribute to the precipitation of REE-phosphates.

Svensk sammanfattning

De sällsynta jordartsmetallerna (på engelska förkortat REE; Rare Earth Elements) är en grupp grundämnen som idag har en nyckelroll i många högteknologiska applikationer inklusive s.k. grön och fossilfri energiteknik. Över tid har flera REE-mineraliseringar konstaterats ha bildats helt eller delvis av hydrotermala fluider (högtempererade vattenlösningar). Hur sådana förekomster kan bildas är ett idag högaktuellt forskningsområde. Den här studien är fokuserad på bildandet av hydrotermala REE-förekomster innehållande REE-fosfaterna monazit [(LREE,Y)PO_4] och xenotim [(Y,HREE)PO_4], två viktiga värdmineral för REE i jordskorpan. Studien inriktar sig främst på att karakterisera de nyupptäckta REE-mineraliseringarna i området kring Olserum-Djupedal utanför Västervik i sydöstra Sverige. Fortsättningsvis undersöks ursprunget av REE och P i dessa förekomster, hur REE och P transporteras i de hydrotermala lösningarna och vilka processer som lett fram till bildandet av monazit och xenotim från dem.

Den primära mineraliseringen i Olserum-Djupedal domineras av samexisterande monazit-(Ce), xenotim-(Y) och REE-förande fluorapatit i gångar huvudsakligen bestående av biotit, magnetit, gedrit och kvarts. Gångarna förekommer i metasedimentära bergarter kring och i kontaktgården till en peraluminös alkalifältspatgranit. Gångarna uppträder även i utkanten av samma granit. Sammantaget visar resultaten att den primära REE-mineraliseringen har ett hydrotermalt ursprung och bildades för omkring 1,8 miljarder år sedan av högtempererade (ca. 600°C) fluider från den närliggande graniten. De primära associationerna omvandlades därefter under avtagande temperatur till ca. 300°C för åtminstone 1,75 miljarder år sedan.

Hydrotermala mineraliseringar med REE-fosfater förknippas vanligtvis med alkalina magmatiska bergarter och karbonatiter eftersom både REE och P i regel uppvisar en stark kemisk affinitet till sådana magmor. Den här studien visar att REE-fosfatförekomster även kan bildas av hydrotermal aktivitet relaterad till magmatiska bergarter av betydligt mindre alkalin karaktär. Av dessa system så har graniter med peraluminös karaktär störst potential att avge fluider anrikade på både REE and P.

Den generella uppfattningen om hur hydrotermala REE-fosfatmineraliseringar har bildats är att REE och P transporterats i separata fluider och att REE-fosfater fällts ut som en konsekvens av att dessa fluider blandats, eller att REE-fosfater bildats som ett resultat av att REE-förande fluider reagerat med fosforrika bergarter. Avsaknaden av fosforrika bergarter i området kring Olserum-Djupedal och förekomsten av samexisterande fluorapatit, monazit-(Ce) och xenotim-(Y) visar dock att sådana scenarier inte nödvändigtvis förklarar alla förekomster av hydrotermala REE-fosfatmineraliseringar. Som ett alternativ kan REE och P ha transporterats i samma fluid. De mest troliga förhållanden för samtransport av REE och P är i fluider med temperaturer som överstiger 400°C och som har höga salthalter. Vidare så gynnar låga pH samtransport av REE och P då olika metallkomplex med REE, exempelvis REE-Cl, REE-F eller REE-SO_4, är väldigt stabila under dessa förhållanden. Samtransport av REE och P är också möjlig vid ett mer neutralt eller basiskt pH. I ett scenario som innefattar samtransport av REE och P så kan pH-förändringar, sänkta temperaturer och destabilisering av viktiga REE-metallkomplex i kombination bidra till utfällning av REE-fosfater.

Sammanfattningsvis kan man säga att i lågtempererade hydrotermala system har REE-fosfaterna sannolikt inte bildats av fluider omfattande samtransport av REE och P, utan genom blandning av två olika fluider eller genom samverkan mellan REE-förande fluider och fosforrika bergarter. I många högtempererade magmatisk-hydrotermala system (> 400°C) så har förmodligen REE och P i REE-fosfaterna däremot haft ett gemensamt ursprung och transporterats i samma fluid.

Acknowledgements

Despite all the hard work in the last couple of years, this PhD journey has been very rewarding and enjoyable. However, my journey would not have been possible without all the support and encouragements I have received during the years. I would like to express my sincere gratitude to all who have helped me in any way.

First, I would like to give a special thanks to my supervisor Thomas Wagner for your support and contribution to this project. Your knowledge in the field, your ability to give swift and helpful feedback and your positive attitude towards my work have helped me in my pursuit to produce high-quality science.

I am grateful that my second supervisor, Erik Jonsson, has been part of the journey. After supervising my M.Sc. thesis, you were the one recommending me and giving me the opportunity to work on this project. Your inputs throughout the years have been vital for my scientific progress and for the outcome of this project.

I wish to thank Tapani Rämö for all your help during the finalising stage of this project. I would further like to express my gratitude to every one part of our former research group at the department (Tobias Fusswinkel, Radoslaw Michallik, Henrik Kalliomäki, Anselm Loges, Dina Schultze, Gabriel Berni and Johan Fredriksson) for your company, support and help. To Tobias, thank you for your friendship and for your willingness to share your knowledge and expertise. To Radek, thanks for your friendship and all your help with the microprobe. To Henrik, thanks for being my office mate for all these years and all our scientific and non-scientific discussions. To Anselm and Dina, thanks for your company and help with various things. To Gabriel, thanks for being my office mate at the beginning of my studies. To Johan, thank you for enabling me to speak some Swedish while at work.

I would like to give my gratitude to Tasman Metals/Leading Edge Materials and especially Johan Berg and Magnus Leijd for your support during fieldwork and for allowing me access to proprietary information. The staff at the NORDSIM facility (Martin Whitehouse, Lev Ilyinsky and Kerstin Lindén) are heartily thanked for the assistance during the SIMS analysis. I further would like to thank the SGU staff at the national drillcore archives in Malå for your valuable help during logging and sampling. Thank you Pasi Heikkilä for your assistance with the microprobe and Helena Korkka for the preparation of thin and thick sections used in this project. Dan Harlov donated reference material for this project, which is greatly acknowledged. The GeoDoc graduate Programme is thanked for providing the additional financial support for international conferences and research visits. My sincere gratitude goes out to all my current and former friends and colleagues at the Department of Geosciences and Geography, who have assisted me in any way and provided me company; thank you!

To my friends and teammates in my table tennis club MBF, thanks for helping me think of something else than work. I am very pleased that I took up this hobby again. Thanks to my family for supporting me and being there for me. Importantly, I would like to end with giving my endless and heartfelt gratitude to my dearest Julia for your ever-lasting support, love and encouragement. I dedicate this thesis to you.

Contents

List of original publications

This thesis is based on the following publications:

I Andersson, S.S., Wagner, T., Jonsson, E., Michallik, R.M., 2018. Mineralogy, paragenesis, and mineral chemistry of REEs in the Olserum-Djupedal REE-phosphate mineralization, SE Sweden. Am. Mineral. 103, 125-142. https://doi.org/10.2138/am-2018-6202

II Andersson, S.S., Wagner, T., Jonsson, E., Fusswinkel, T., Leijd, M., Berg, J.T., 2018. Origin of the high-temperature Olserum-Djupedal REE-phosphate mineralisation, SE Sweden: A unique contact metamorphic-hydrothermal system. Ore Geol. Rev. 101, 740-764. https://doi.org/10.1016/j.oregeorev.2018.08.018

III Andersson, S.S., Wagner, T., Jonsson, E., Fusswinkel, T., Whitehouse, M.J., 2019. Apatite as a tracer of the source, chemistry, and evolution of ore-forming fluids: the case of the Olserum-Djupedal REE-phosphate mineralisation, SE Sweden. Accepted for publication in Geochimica et Cosmochimica Acta. https://doi.org/10.1016/j.gca.2019.04.014

The publications are referred to in the text by their Roman numerals.

Author's contribution to the publications

I This study was initially planned by T. Wagner and E. Jonsson but revised by T. Wagner, E. Jonsson, and S.S. Andersson. Sampling was mainly conducted by S.S. Andersson with assistance from T. Wagner and E. Jonsson. Petrographical/textural analysis and EPMA and LA-ICP-MS analyses were performed by S.S. Andersson. Analytical EPMA protocols were co-developed by S.S. Andersson and R.M. Michallik. Results were interpreted jointly by S.S. Andersson, T. Wagner, and E. Jonsson. S.S. Andersson prepared the manuscript with contributions from the co-authors.

II This study was initially planned by T. Wagner and E. Jonsson but revised by T. Wagner, E. Jonsson, and S.S. Andersson. Fieldwork and sampling were mainly conducted by S.S. Andersson with assistance from T. Wagner, E. Jonsson, M. Leijd and J. Berg. Petrographical/textural analysis, EPMA and LA-ICP-MS were performed by S.S. Andersson. T. Fusswinkel assisted with LA-ICP-MS analysis. The results were interpreted jointly by S.S. Andersson, T. Wagner, and E. Jonsson. The manuscript was prepared by S.S. Andersson with contributions from the co-authors.

III This study was designed by T. Wagner, E. Jonsson, and S.S. Andersson. Selection of samples and analyses by EPMA, SIMS, and LA-ICP-MS were performed by S.S. Andersson. Analytical protocols for EPMA and LA-ICP-MS were developed by S.S. Andersson. M. Whitehouse assisted with SIMS analysis and T. Fusswinkel with LA-ICP-MS analysis. Results were interpreted jointly by S.S. Andersson, T. Wagner, E. Jonsson, and T. Fusswinkel. S.S. Andersson prepared the manuscript with contributions from the co-authors.

Abbreviations

BSE	Back-scattered electrons
EPMA	Electron-probe micro-analysis
FIA	Fluid inclusion assemblage
HFSE	High-field strength elements
LA-ICP-MS	Laser-ablation inductively coupled plasma mass spectrometry
REE	Rare earth elements
SIMS	Secondary ion mass spectrometry
TIB	Transscandinavian igneous belt

List of tables and figures

1 Introduction

The scientific interest in the rare earth elements (REE) has always been strong. With the increasing recognition that the REE can be mobile in certain hydrothermal fluids, recent geochemical modelling has highlighted how the REE behave in hydrothermal systems, i.e., how REE are transported in aqueous solutions and what controls the precipitation of REE (e.g., Migdisov and Williams-Jones, 2014; Migdisov et al., 2016; 2018; Perry and Gysi, 2018). These models are based on experimental data, and it is thus important to test and compare them to how REE behave in natural hydrothermal systems. This study explores the key processes and system parameters that are important for the formation of hydrothermal REE deposits rich in the REE-phosphates monazite [(LREE,Y)PO_4] and xenotime [(Y,HREE)PO_4]. This is done by studying the Olserum-Djupedal REE mineralisation in south-eastern Sweden. This is an exceptional example of a hydrothermal REE system dominated by monazite-(Ce), xenotime-(Y) and fluorapatite, thus providing a unique opportunity to study how REE and P behave in hydrothermal systems.

1.1 The REE; what are they?

The REE include the 15 lanthanides (Z = 57 to 71, La to Lu) and Y (Z = 39; Table 1). Scandium (Z = 21) is officially also included in this definition by the International Union of Pure and Applied Chemistry (IUPAC; e.g., Gupta and Krishnamurthy, 2005; Wall, 2014), although commonly excluded from the REE when discussing geological processes. Contrary to what the term "rare earth" may imply, the REE are not particularly rare in nature. This term was given because of the extreme difficulties in chemically separating the elements from one and other and to signify the stable nature of the REE as oxides (termed "earths") rather than metals (Wall, 2014). The challenge in separating the elements is reflected in the extended period it took to isolate them. The first REE to be isolated, or more accurately, the first "earth", was "yttria" by the Finnish chemist J. Gadolin in 1794 from the mineral gadolinite [$(REE,Y)_2Fe^{2+}Be_2O_2(SiO_4)_2$] from the Ytterby pegmatite in Sweden (Gupta and Krishnamurthy, 2005). From the Bastnäs mines in Sweden, it was realised in the same time period that another mineral (cerite; [$Ce_9(Mg,Fe)(SiO_4)_6(SiO_3OH)(OH)_3$]) was found to contain the REE, and in 1804, "ceria" was separated. However, it was soon realised that "yttria" and "ceria" were mixtures of several REE. From "yttria" and "ceria", all REE were finally discovered by 1907 (Gupta and Krishnamurthy, 2005; Wall, 2014). Promethium was not verified until 1945 (Gupta and Krishnamurthy, 2005), because of its very short half-life; the most stable isotope ^{145}Pm has a half-life of 17.7 years (Audi et al., 2003).

The difficulties in separating the REE stem from the very similar physical and chemical properties exhibited by the individual REE (excluding Sc). This mainly originates from the similar electronic configuration of the REE (Table 1). The lanthanides are part of the f-block of elements together with the actinides. Starting from Ce, the inner transition 4f electron shells in the atoms are subsequently filled towards Lu. Lanthanum is technically not a lanthanide (the term means lanthanum-like) due to the lack of 4f electrons (Gupta and Krishnamurthy, 2005). Because of the shape of the seven inner 4f-orbitals, they exert only a weak shielding effect on the valence electrons from the positive nucleus charge. Thus, with increasing atomic number, the effective nuclear charge increases, and the valence electrons are more strongly pulled towards the nucleus. This result in a steady reduction in the atomic and ionic

Table 1. List of the REE, some properties and their applications. Table compiled from Shannon (1976), McDonough and Sun (1995), Rudnick and Gao (2003), Gupta and Krishnamurthy (2005), and Navarro and Zhao (2014).

Element	Symbol	Z	Atomic weight	Electron configuration (atomic)	Electron configuration (ionic)	Effec-tive ionic radius (Å)	Upper crust abundance (ppm)	C1 Chondrite abundance (ppm)	Applications/uses
Scandium	Sc	21	44.96	[Ar] $4s^2$ $3d^1$	[Ar] (3+)	0.87 (3+)	14	5.92	Aerospace materials, consumer electronics, lasers, magnets, lightning, sporting goods
Yttrium	Y	39	88.91	[Kr] $5s^2$ $4d^1$	[Kr] (3+)	1.075 (3+)	21	1.57	Ceramics, communication systems, LED, lightning, frequency meters, fuels additive, jet engine turbines, televisions, microwave communica-tions, satellites, vehicle oxygen sensors
Lanthanum	La	57	138.91	[Xe] $6s^2$ $5d^1$	[Xe] $4f^0$ (3+)	1.216 (3+)	31	0.237	Compact fluorescent lamps, catalyst in petroleum refining, television, energy storage, fuel cells, night vision instruments, rechargeable batter-ies
Cerium	Ce	58	140.12	[Xe] $6s^2$ $4f^1$ $5d^1$	[Xe] $4f^1$ (3+), [Xe] $4f^0$ (4+)	1.196 (3+), 0.97 (4+)	63	0.613	Catalytic converters, catalyst in petroleum refining, glass, diesel fuel additive, polishing agent, pollution-control systems
Praseodymium	Pr	59	140.91	[Xe] $6s^2$ $4f^3$	[Xe] $4f^2$ (3+)	1.179 (3+)	7.1	0.0928	Aircraft engine alloy, airport signal lenses, catalyst, ceramics, colour-ing pigment, electric vehicles, fibre optic cables, lighter flint, magnets, wind turbines, photographic filters, welder's glasses
Neodymium	Nd	60	144.24	[Xe] $6s^2$ $4f^4$	[Xe] $4f^3$ (3+)	1.163 (3+)	27	0.457	Anti-lock brakes, air bags, anti-glare glass, cell phones, computers, electric vehicles, lasers, MRI machines, magnets, wind turbines
Promethium	Pm	61	144.91	[Xe] $6s^2$ $4f^5$	[Xe] $4f^4$ (3+)				Beta source for thickness gases, lasers for submarines, nuclear-pow-ered battery
Samarium	Sm	62	150.36	[Xe] $6s^2$ $4f^6$	[Xe] $4f^5$ (3+)	1.132 (3+)	4.7	0.148	Aircraft electric systems, electronic counter measure equipment, electric vehicles, flight control surfaces, missile and radar systems, optical glass, permanent magnets, precision guided munitions, stealth technology, wind turbines
Europium	Eu	63	151.96	[Xe] $6s^2$ $4f^7$	[Xe] $4f^7$ (2+), [Xe] $4f^6$ (3+)	1.300 (2+), 1.12 (3+)	1	0.0563	Compact fluorescent lamps, lasers, LED, television screens (CRT, LCD, Plasma), tag complex for the medical field
Gadolinium	Gd	64	157.25	[Xe] $6s^2$ $4f^7$ $5d^1$	[Xe] $4f^7$ (3+)	1.107 (3+)	4	0.199	Computer data technology, magneto-topic recording technology, microwave applications, MRI machines, power plant radiation leaks detector
Terbium	Tb	65	158.93	[Xe] $6s^2$ $4f^9$	[Xe] $4f^8$ (3+)	1.095 (3+)	0.7	0.0361	Compact fluorescent lamps, electric vehicles, fuel cells, televisions, optic data recording, permanent magnets, wind turbines
Dysprosium	Dy	66	162.5	[Xe] $6s^2$ $4f^{10}$	[Xe] $4f^9$ (3+)	1.083 (3+)	3.9	0.246	Electric vehicles, home electronics, lasers, permanent magnets, wind turbines
Holmium	Ho	67	164.93	[Xe] $6s^2$ $4f^{11}$	[Xe] $4f^{10}$ (3+)	1.072 (3+)	0.83	0.0546	Microwave equipment, colour glass
Erbium	Er	68	167.26	[Xe] $6s^2$ $4f^{12}$	[Xe] $4f^{11}$ (3+)	1.062 (3+)	2.3	0.16	Colour glass, fibre optic data transmission, lasers
Thulium	Tm	69	168.93	[Xe] $6s^2$ $4f^{13}$	[Xe] $4f^{12}$ (3+)	1.052 (3+)	0.3	0.0247	X-ray phosphors
Ytterbium	Yb	70	173.04	[Xe] $6s^2$ $4f^{14}$	[Xe] $4f^{13}$ (3+)	1.042 (3+)	1.96	0.161	Improving stainless steel properties, stress gages
Lutetium	Lu	71	174.97	[Xe] $6s^2$ $4f^{14}$ $5d^1$	[Xe] $4f^{14}$ (3+)	1.032 (3+)	0.31	0.0246	Catalysts, positron emission tomography (PET) detectors

size, which is termed the lanthanide contraction (Gupta and Krishnamurthy, 2005; Wall, 2014). The magnitude of this effect becomes stronger for the heavy rare earth elements (HREE), thus approaching similar atomic and ionic sizes as Y. This readily explains the common association of Y with the HREE, and why Y usually is placed between Dy and Ho in normalised REE distribution patterns.

The 4f-electrons also govern the magnetic behaviour of the REE. Excluding REE lacking these electrons (Sc, Y, and La) and those that have filled 4f-shells (Yb and Lu), the REE are strongly paramagnetic and becomes antiferromagnetic or ferromagnetic at lower temperatures. Gadolinium(III) exhibits the highest magnetic moment because it can have 7 unpaired electrons in the f-shell, and is therefore used in magnetic resonance imaging (MRI) techniques. Samarium in alloys with cobalt (SmCo5) create strong magnets with high coercivity (a measure of a material's resistance to becoming demagnetised). However, Nd in alloy with Fe and B ($Nd_2Fe_{14}B$) create even stronger magnets. Because of Nd being the 3rd most abundant REE and Fe being readily available (compared to Co), these strong Nd-magnets are now widely used in a variety of applications, such as in electric motors for the electric car industry and in generators in wind turbines, or in applications requiring small but strong magnets such as in hard drives and smartphone speakers (Table 1; Gupta and Krishnamurthy, 2005). Dysprosium is also used as a key dopant in the Nd magnets to increase the coercivity and the high-temperature performance.

The REE mostly occur in nature in a trivalent state but can also occur as divalent or tetravalent ions because of the strive to attain empty, half-filled or filled f-shell configurations. For instance, Ce may occur as (IV) because it can obtain an empty f-shell, whereas Eu commonly occurs as (II) as it can attain a half-filled f-shell configuration (Table 1). The trivalent ions, excluding Ce^{3+} and Yb^{3+}, display very sharp absorption-emission bands in the ultraviolet and visible light spectrum resulting from f-f-electron transitions (Gupta and Krishnamurthy, 2005). This has been utilised in several applications, for example, in colouring or decolouring glass or ceramics. More technical applications include the REE as doping agents or activators in crystals (for example Nd-doped Yl-Al-garnet, Nd:YAG) so they can be used as solid-state lasers. These are widely used for cutting procedures in medical applications, or cutting, welding and marking metals, or as the laser source in laser-ablation techniques. The REE are also commonly used as phosphors, i.e., materials that exhibit luminescence, for video display screens (CRT, plasma, LCD), fluorescent lights and LED, amongst others.

The REE are classified as critical metals (particularly Nd, Eu, Dy, Tb, and Y) for modern-day industrial and green-energy applications (Goodenough et al., 2016; Paulick and Machacek, 2017, and references therein). The global production of REE doubled from 1994 (65000 t) to 2010 (130000 t), while today's numbers are around 120000 t (Weng et al., 2015; Paulick and Machacek, 2017). China has been the dominating supplier following the loss of other actors from the market in the late 1990s (e.g., USA and Australia amongst others), and today, at least 85% of the REE are supplied by China, mainly from the giant Bayan Obo deposit. Following the global REE price peak in 2011 as a result of export restrictions from China and domestic ambitions, the price of REE has dropped back to levels prior to the boom, and other producers than China have again entered the market, like USA (Mountain Pass), Australia (Mt. Weld) and Russia (Lovozero). From the exploration boom, the defined REE mineral resources outside of China more than doubled from 40 Mt (2011) to 98 Mt (2016; Paulick and Machacek, 2017). The

global total rare earth oxide (TREO) resources are estimated to about 165 Mt, which would be enough to cover hundreds of years of the demand of REE at present yearly consumption rates (120000 t; Paulick and Machacek, 2017). However, the demand for the most critical REE is estimated to increase at a rate of approximately 5-10% per year, albeit with some caveats (Hatch, 2012; Massari and Ruberti, 2013), because of the expanding use of REE in current and future technologies (Wall, 2014). There are also few substitutes for some of the REE (Wall, 2014). The vulnerability of China being the major actor in the market is a strong incentive to study how the REE behave in geological systems.

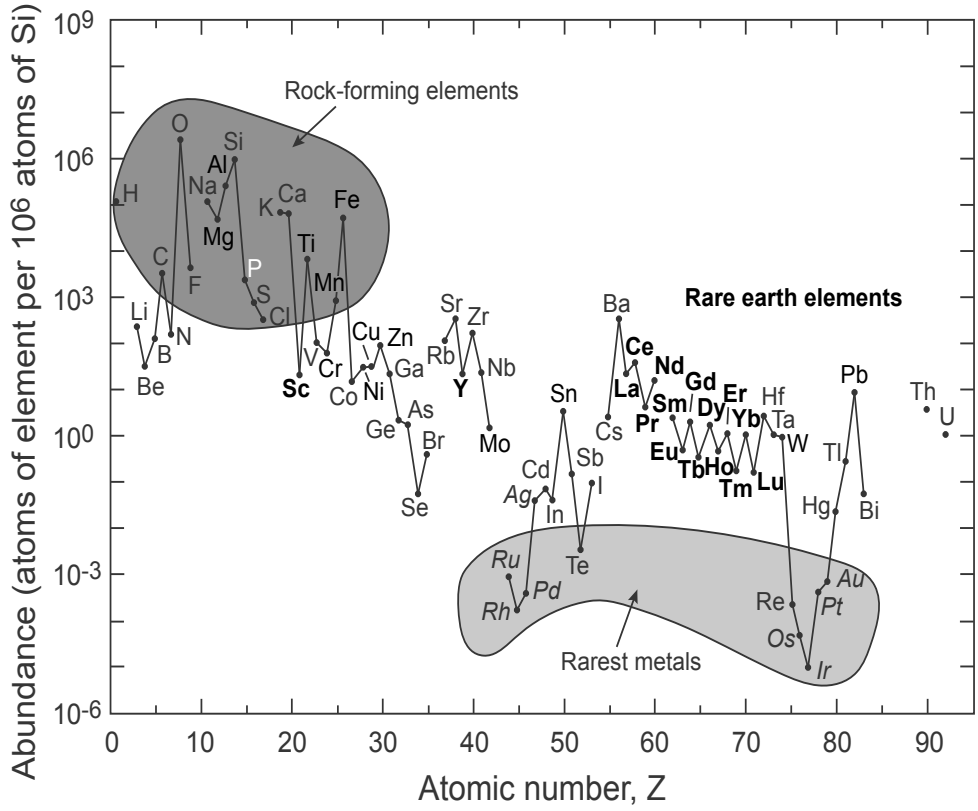

Fig. 1. Crustal abundance of chemical elements as a function of atomic number. Modified from Haxel et al. (2002).

1.2 Hydrothermal REE deposits

The REE are lithophile elements, i.e., they are enriched in the crust (Castor and Hendrick, 2006). The REE have a similar crustal abundance as Cu and Zn down to that of Bi and are more abundant than the precious metals Au and Pt (Fig. 1; Table 1). Light rare earth elements (LREE; from La to Sm) are more abundant than the heavy rare earth elements (HREE; from Eu to Lu). REE with even atomic numbers are more abundant than those with odd atomic numbers because of the Oddo Harkins effect (North, 2008).

The REE are typically disseminated in the Earth's crust and rarely enriched in high concentrations. When they do occur in higher concentrations, they make up a REE mineralisation. If the REE concentrations are high enough so that REE extraction is economically feasible, they constitute a REE deposit. The enrichment of REE to form REE deposits can occur through primary

processes such as from magmatism or hydrothermal (re-)mobilisation, or by secondary processes such as weathering and by gravity separation during sedimentary processes. Hydrothermal REE deposits are those that have formed dominantly by hydrothermal processes; i.e., REE-minerals precipitated from hot aqueous solutions (hydrothermal fluids). Most of the hydrothermal REE deposits form in association with magmatism of different chemical affinity, from alkaline to peralkaline granites and syenites (e.g., Strange Lake, Canada; Gysi and Williams-Jones, 2013; Vasyukova et al.; 2016), to carbonatites (e.g., Lofdal, Namibia; Wall et al., 2008; Bodeving et al., 2017), to peralkaline agpaitic rocks (e.g., Nechalacho, Canada; Möller and Williams-Jones, 2016, 2017), and seldom with subalkaline granitic or granitoid rocks (e.g., Kutessay II, Kyrgyzstan, Djenchuraeva et al., 2008). Iron-oxide copper-gold (IOCG) deposits, although likely associated with magmatism as well, are mostly mined for Cu or Au but can sometimes contain high concentrations of REE (e.g., Olympic Dam, Australia; Schmandt et al., 2017).

Excluding REE deposits associated with peralkaline systems, in which REE mostly are hosted in REE silicates or oxides (e.g., gadolinite, fergusonite [(REE,Y)(Nb,Ti)O_4] and allanite [$(Ca,REE,Y)_2(Al,Fe)_3(SiO_4)Si_2O_7)O(OH)$]) and primary magmatic zircon- and titanosilicates (e.g., eudialyte [$Na_{15}Ca_6Fe_3Zr_3Si(Si_{25}O_{73})(O,OH,H_2O)_3(Cl,OH)_2$]), common REE-bearing minerals in most hydrothermal systems are the REE-phosphates monazite [(LREE,Y)PO_4] and xenotime [(Y,HREE)PO_4], and the REE-fluorocarbonates, chiefly bastnäsite [(REE,Y)CO_3F]. The REE-phosphates can be the principal REE-bearing minerals in deposits associated with carbonatites (e.g., Ashram, Canada, Mitchell and Smith, 2017; Fen, Norway, Andersen, 1986; Marien et al., 2018; Lofdal, Namibia, Williams-Jones et al., 2015), in granitic-hydrothermal deposits (Kutessey II, Kyrgyzstan; Djenchuraeva et al., 2008), in IOCG deposits (e.g., Lala, China; Chen and Zhou, 2015), and in vein-type REE-Th deposits in USA (Diamond Creek and Lemhi Pass; Long et al., 2010). In many of these deposits, monazite-(Ce) or monazite-(Nd) is the dominating REE-phosphate. Importantly, a rather newly recognised group with xenotime-(Y) as the principal mineral is unconformity-related REE deposits, which show a similar geological environment and formation conditions as unconformity-related uranium deposits (e.g., Maw Zone in the Athabasca Basin, Canada; Rabiei et al., 2017; Wolverine, Killi Killi Hills and John Gault deposits, Australia; Vallini et al., 2007; Richter et al., 2018; Nazari-Dehkordi et al., 2018).

1.3 Hydrothermal transport of REE and P

Prerequisites for the formation of hydrothermal REE deposits rich in the REE-phosphates are: 1) significant transport of REE and P in hydrothermal fluids, either together or in separate fluids and 2) efficient precipitation mechanisms to remove the REE, and in part, P, from the fluid(s). Transport of REE in a fluid requires the formation of stable metal complexes with available ligands (anion species) in the fluid at the specific conditions of the hydrothermal system to keep the REE in solution. A variety of ligands occur in natural systems, such as Cl^-, F^-, SO_4^{2-}, OH^-, CO_3^{2-}, and PO_4^{3-}. As a first approximation, based on the HSAB (Pearson's hard/soft acid/base) principle, REE are hard cations (high charge and small ionic radius) and should form stable complexes with hard ligands such OH^-, F^-, CO_3^{2-}, and SO_4^{2-}, and less stable complexes with the borderline ligand Cl^- (Williams-Jones and Migdisov, 2014). Indeed, experimental studies have demonstrated that the dominant REE-F complexes are two to three orders more stable than the dominant REE-

Cl complexes (Migdisov et al., 2009). However, the ability to form stable complexes is not the only important factor in controlling the transport of REE. This depends strongly on the activity or the concentration of the specific ligand in the system, and if the specific ligand is bounded or not to other aqueous species present in the fluid. This is in turn strongly dependent on the solubility of the REE mineral containing this specific ligand because the mineral will act as a buffer of the REE concentrations in the fluid. A more insoluble REE-mineral can buffer the REE to rather low concentrations. The availabilities of ligands also depend on pH and temperature. Hydrochloric acid (HCl) is a strong acid and at temperatures up to 300-400 °C, HCl is largely dissociated and occurs as the free ions H^+ and Cl^- at a pH higher than 2. At even higher temperatures, HCl can even be largely associated at acidic conditions. However, hydrofluoric acid (HF) is a weaker acid and depending on temperature, only at near-neutral and alkaline pH does HF occur as the free dissociated ions H^+ and F^- (Migdisov and Williams-Jones, 2014). Thus, at near-neutral to alkaline conditions, more F ions are available to bind with the REE, but this also coincides with a reduction of the solubility of the REE-fluoride mineral and the REE concentration in the fluid drops. However, the involvement of stable REE-OH complexes at higher pH may oppose the buffering effect the REE-fluorides have on the REE concentrations, and the fluid may retain high concentrations of REE even at higher pH conditions.

The solvent, H_2O, is also important because, with increasing temperature and decreasing pressure, the degree of hydrogen bonding decreases (dielectrical constant decreases). This explains why metals occur dominantly as simple cations in solutions at ambient conditions whereas, at elevated temperatures, metals form complexes because of strong ion-pairing (stronger electrostatic attraction between charged ions). This also means that Cl^- forms stable ion-pars with Na^+ and K^+, cations common in hydrothermal fluids, at elevated temperatures, thus decreasing the availability of Cl^- ions. However, $NaCl^\circ$ and KCl° complexes are relatively weak compared to the REE complexes at higher temperatures, thus compensating for the reduced Cl activity and promoting REE complexing with increasing temperature (Williams-Jones and Migdisov, 2014).

The most common ligand in hydrothermal fluids is Cl^-. Experimental studies have shown that the mono- and dichloride species, $REECl^{2+}$ and $REECl_2^+$, are the dominating REE-Cl species up to 300 °C. The overall stabilities of the REE-Cl complexes increase with temperature and the complexes with LREE are more stable than with HREE, an effect that is accentuated at higher temperatures (Migdisov et al., 2009; 2016).

REE complexes involving F^- were early believed to be the major REE-transporting agent in hydrothermal fluids because REE form very stable complexes with F compared to Cl. This was mainly based on early theoretical predictions, which showed an increased mobility of the REE along the lanthanide series (increasing stabilities of REE-F complexes; Wood, 1990; Haas et al., 1995). This increase in stabilities of REE-F complexes follows the HSAB principle because the data were extrapolated from ambient conditions. Because F^- is a hard ligand, and the REE become increasingly harder along the lanthanide series (ionic radius decreases), the stabilities of REE-F complexes should increase with increasing atomic number, which is the case at ambient temperatures (Williams-Jones et al., 2012). However, at elevated temperatures, the decreased hydrogen-bonding ability of H_2O enables electron transfer and "softening" of ions. Thus, F^- is much softer at elevated temperatures than at ambient conditions, which will result in that the increase in REE-F complex stabilities along the

series should be weaker or even reversed. This also explains why HREE-Cl relative to LREE-Cl complexes are much weaker at elevated temperatures than at ambient conditions (because Cl^- is much softer; Williams-Jones et al., 2012).

Experimental studies show that the stabilities of the REE-F complexes mostly decrease along the series at elevated temperatures (> 150 °C) and that they are overall less stable than predicted theoretically, which conforms to the above theory of "softening" of ions (Migdisov et al., 2009; 2016). At ambient temperatures and up to 100 °C, $REEF^{2+}$ and $REEF_2^+$ are the dominant species. Above 100 °C, $REEF^{2+}$ is the only dominant species, and its stability increases with temperature (Migdisov et al., 2009). Experimental work on Y shows that at low temperature (100 °C), YF_2^+ dominates, whereas Y^{3+} and YF^{2+} are the dominant species at low and high F activity at temperatures up to 250 °C (Loges et al., 2013).

Phosphorous in aqueous solutions mostly occurs as phosphoric acid ($H_3PO_4^\circ$) and the dissociated acids $H_2PO_4^-$, HPO_4^{2-} or PO_4^{3-}, or as polyphosphoric acids and their dissociated ions (e.g., $H_4P_2O_7^\circ$ and $H_3P_2O_7^-$) depending on temperature, pH and activity of P (Pourtier et al., 2010). The stabilities of phosphate complexes with the REE have not been studied at hydrothermal conditions. Because $H_2PO_4^-$, HPO_4^{2-} and PO_4^{3-} are hard ligands, REE form stable complexes ($REEH_2PO_4^{2+}$, $REEHPO_4^+$, REEPO4) with them at ambient temperatures (Haas et al., 1995; Williams-Jones and Migdisov, 2014). In contrast to REE complexation with $H_2PO_4^-$, complexation of REE with HPO_4^{2-} and PO_4^{3-} should also only occur at high pH conditions because H_3PO_4 is a weak acid. Thus, at low pH, only strongly protonated forms of the ligands occur ($H_3PO_4^\circ$ and $H_2PO_4^-$). A limiting factor for significant REE transport by phosphate complexing is the low solubilities of monazite and xenotime. The solubilities of monazite and xenotime are retrograde up to 300 °C (solubility decreases with increasing temperature; Poitrasson et al., 2004; Cetiner et al., 2005; Gysi et al., 2015; 2018). However, another recent study suggests a prograde solubility (increases with temperature) of monazite from 300 °C up to 800 °C (Pourtier et al., 2010), which may indicate that REE-P complexing may be important at higher temperatures, or that phosphate is co-transported with REE in the fluid and the REE are complexed with other ligands.

Other potential ligands in hydrothermal fluids include SO_4^{2-}, OH^-, CO_3^{2-}, and HCO_3^-. The REE-sulphate complexes are more stable than REE-Cl complexes, but not as stable as REE-F complexes. The dominating species are $REESO_4^+$ and $REE(SO_4)^{2-}$, and experimental studies show that they become increasingly stable at increasing temperatures (Migdisov and Williams-Jones, 2008). The hydroxyl group (OH^-) forms stable complexes with the REE at high pH conditions. The principal species are $REE(OH)_3^\circ$, $REE(OH)^{2+}$, and $REE(OH)_2^+$. At elevated temperatures (290 °C), all three species are important, in addition to the simple hydrated REE^{3+} ion, which dominates at low pH. There is also an increase in stability with temperature (Wood et al., 2002). The carbonate (CO_3^{2-}) or bicarbonate (HCO_3^-) ligands form stable complexes with the REE ($REECO_3^+$ and $REEHCO_3^{2+}$) consistent with the HSAB principle. No experimental studies have been conducted up to this point, and the data at hydrothermal conditions originates from the theoretical predictions (Wood, 1990; Haas et al., 1995). These show that the stabilities increase with temperature and that the $REECO_3^+$ species is overall the stronger complex. In organic-rich fluids, carboxylates such as acetate (CH_3COO^-) and propanoate ($CH_3CH_2COO^-$) may be important REE transporting ligands (Lecumberri-Sanchez et al., 2018).

1.4 Objectives of the study

The main objectives of this study were:

1) By using a multi-analytical approach, comprehensively characterise the hydrothermal REE mineralisation in the Olserum-Djupedal district. This included detailed studies on the mineralogy, paragenetic evolution and mineral-chemistry of the REE-bearing minerals and the gangue minerals (Papers I, II, and III), characterisation of the style of mineralisation and field relationships (Paper II), and identification of the source and evolution of the hydrothermal fluids (Papers II and III).

2) Based on the findings from the papers, evaluate different sources of REE and P in hydrothermal REE-phosphate deposits and discuss how REE and P are transported in fluids, and compare this to models of hydrothermal transport of REE (and P) based on experimental studies. Ultimately, the aim is to define conditions that are imperative for the formation of hydrothermal deposits rich in REE-phosphates.

2 Geological background

2.1 Regional Geology

The studied Olserum-Djupedal REE-phosphate mineralisation is located in the Olserum-Djupedal district, which comprises three main mineralised areas; Olserum, Bersummen, and Djupedal. The Olserum-Djupedal district is situated NW of the city of Gamleby in the Västervik region, close to the border between the Palaeoproterozoic Västervik metasedimentary Formation and the Transscandinavian Igneous Belt (TIB) and just south of the Svecofennian domain (Fig. 2; Gavelin, 1984; Gaál and Gorbatchev, 1987, Gorbatchev, 2004). The Svecofennian domain formed by an accretionary-type orogeny at 1.92-1.77 Ga. This unit is bordered in the west and south by the large, NNW-SSE trending plutonic and subvolcanic TIB complex, which formed along an active continental margin between 1.85 and 1.65 Ga (Gorbatchev, 2004).

The Västervik Formation consists of meta-supracrustal rocks, mainly quartzites, and meta-arenites and minor meta-argillites and metavolcanic rocks, deposited between c. 1.88 and 1.85 Ga within an extensional tectonic regime (Gavelin, 1984; Beunk and Page, 2001; Bergström et al., 2002; Sultan et al., 2005). Subsequently, magmatic rocks of various geochemical and tectonic affinity intruded the metasupracrustal unit. These have traditionally been referred to as consisting of an older, c. 1.85 Ga deformed augen gneiss and younger, c. 1.81-1.77 Ga granitoids of the TIB-1 suite (Gavelin 1984; Kresten, 1986; Åhäll and Larsson, 2000; Andersson and Wikström 2004). Nolte et al., (2011) and Kleinhanns et al. (2015) recently proposed a new tectono-magmatic model for the Västervik region based on new zircon U-Pb age data, and new petrographical and geochemical classification of the granitoids. According to this model, deposition of the Västervik sediments first occurred in a back-arc environment between 1.88-1.85 Ga followed by ferroan magmatism at around 1.85 Ga. During 1.85-1.81 Ga, a compressional regime was prevalent featuring the intrusion of Cordilleran-type (or magnesian) granitoids. These comprise most of the magmatic rocks in the region. This stage was followed by an extensional or transtensional regime with the intrusion of moderately shallow, mostly peraluminous ferroan anatectic granites at or slightly after 1.8 Ga. A series of syn- and anticlines trending NW and SE comprise the main structural fabrics in the Västervik Formation (Gavelin, 1984), and are presumably pre- to syn-kinematic with the emplacement of the youngest anatectic granites (Westra et al.,

1969; Elbers, 1971).

The Västervik region hosts a variety of Fe ± U ± REE mineralisations (Uytenbogaardt, 1960; Welin, 1966a, 1966b; Hoeve, 1974, 1978), but is mostly known for the occurrence of various types of Cu ± Mo ± Co ± Fe mineralisations, e.g., the Gladhammar deposit (Tegengren, 1924; Uytenbogaardt, 1960; Sundblad, 2003; Billström et al., 2004). Three types of U ± REE mineralisations have been recognised (Uytenbogaardt, 1960): 1) quartzite-hosted heavy mineral-rich palaeobeds (palaeoplacers) containing uraninite and thucholite, 2) magnetite ore with U ± REE minerals; and 3) U ± REE minerals in pegmatites and aplites. Previous interpretations of the three types of U ± REE mineralisations include: 1) magmatic origin (Uytenbogaardt, 1960); 2) palaeoplacer origin remobilised during the intrusion of the younger anatectic granites (Welin, 1966a, 1966b); or 3) hydrothermal origin linked with Na ± Ca alteration and formation of distinct quartz-plagioclase rocks (Hoeve, 1974, 1978).

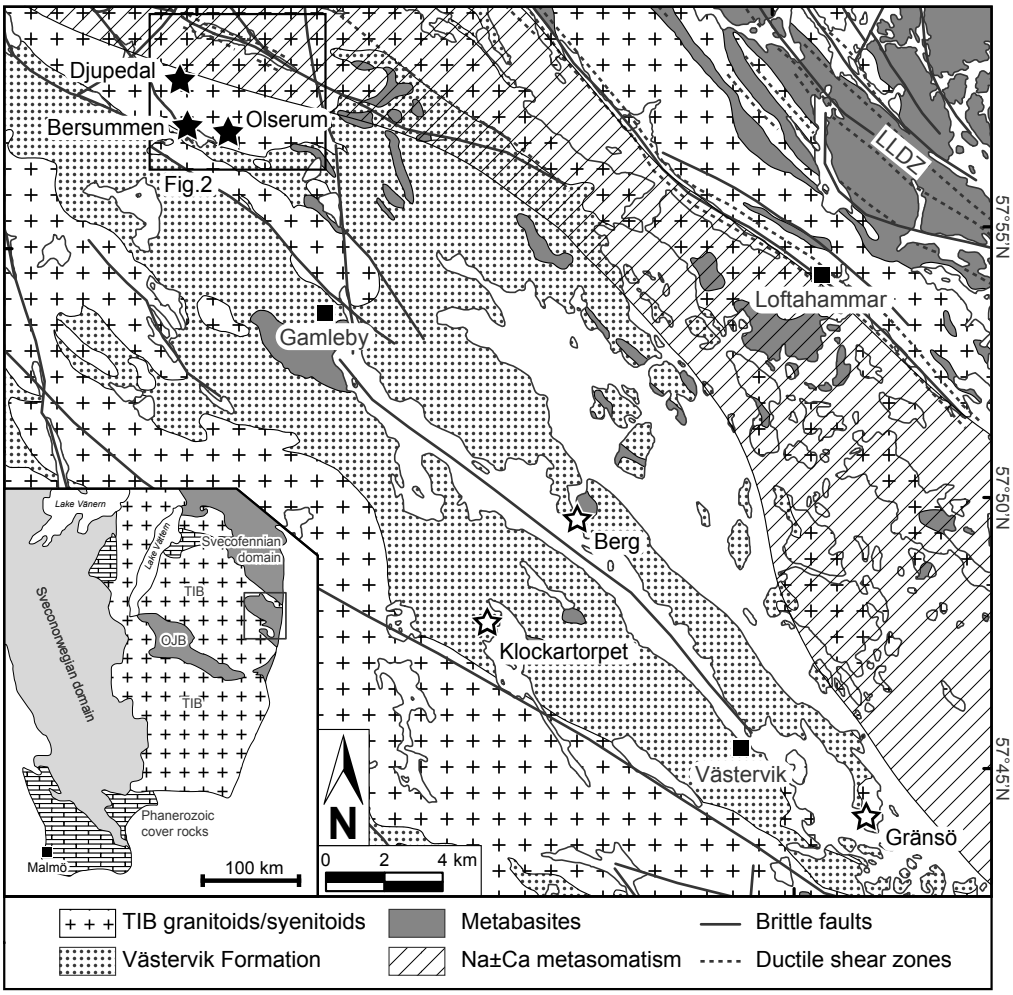

Fig. 2. Geological map of the Västervik region with black stars indicating the location of the exposed REE mineralised areas. Open stars represent locations of supplementary samples. The lower-left inset map portrays the regional geology of southern Sweden, redrawn from Andersen et al. (2009). LLDZ: Loftahammar-Linköping Deformation Zone (Beunk and Page, 2001); TIB: Transscandinavian Igneous Belt (Gorbatschev, 2004); OJB: Oskarshamn-Jönköping Belt (Mansfeld et al., 2005).

2.2 Geology of the Olserum-Djupedal district

Detailed geological mapping in the Olserum-Djupedal district prior to this study is lacking. This section is thus based on field mapping conducted during this study (Paper II). The dominant rock type in the district is a ferroan, peraluminous, calc-alkalic to alkali-calcic, alkali-feldspar TIB granite with an age about 1.8 Ga (Fig. 3). Metasedimentary REE-bearing rocks (Olserum-Djupedal metasediments) are exposed in an ESE-WNW trending zone in the contact zone between the alkali-feldspar granite and the rocks of the Västervik Formation. Similar metasedimentary REE-bearing rocks are also exposed in the Bersummen area and as larger migmatised REE-bearing metasedimentary bodies farther NW in the Djupedal area. The metasedimentary rocks are non-foliated to gneissic whose fabric is trending roughly NW to SE. Feldspar-porphyritic TIB intrusions occupy the area to the north of the Olserum-Djupedal REE mineralisation (Fig. 3). Characteristic white quartz-plagioclase rocks formed by Na ± Ca metasomatism, similar to those described by Hoeve (1974, 1978), are widespread in an area north of the Djupedal area (Fig. 3).

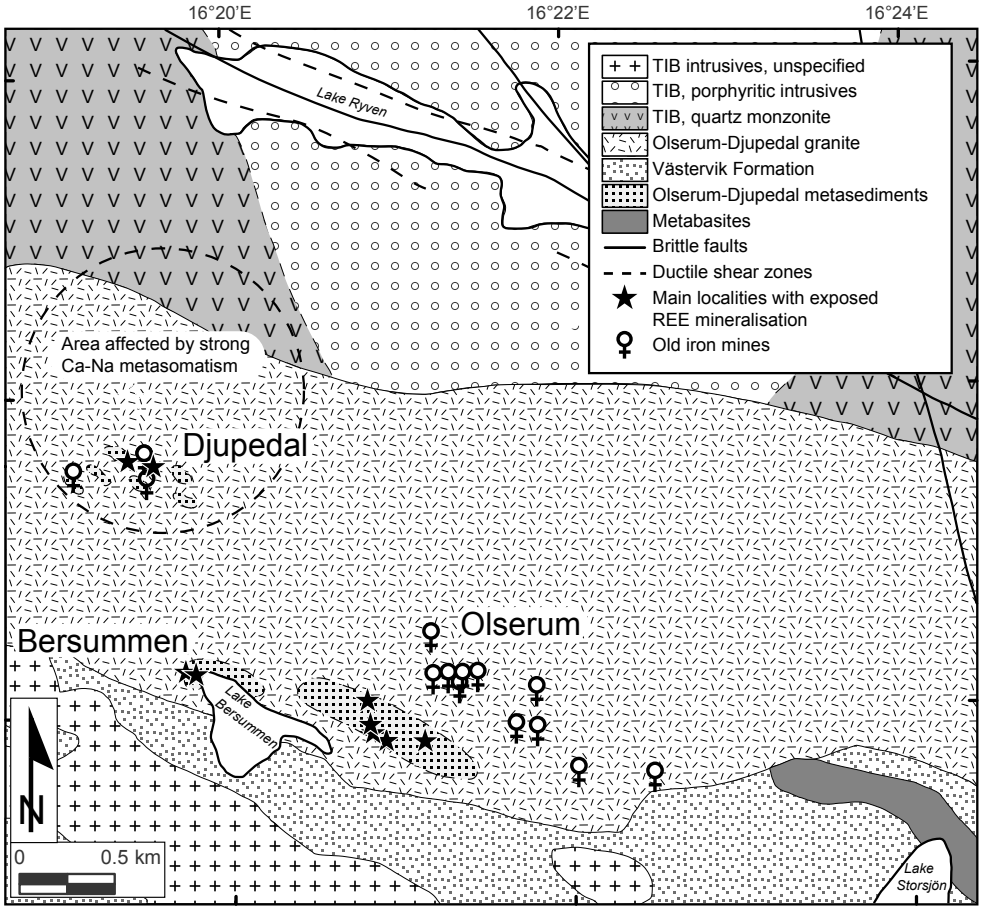

Fig. 3. A simplified geological map of the Olserum-Djupedal district. Modified after Paper II.

3 Analytical methods

3.1 Sampling and field work

Samples for the study (papers I, II and III) were all collected during 2015 and 2016. Samples were both obtained from drill cores drilled by Tasman Metals Ltd. and stored at the archives of the Geological Survey of Sweden in Malå and from surface sampling during field mapping in 2015 and 2016. Sampling was targeted to obtain a representative suite of samples of the REE mineralisations and the host rocks. Field mapping was conducted to get an understanding of the style and timing of the REE mineralisation in the Olserum-Djupedal district. Additional sampling and field mapping from other occurrences in the Västervik region (Klockartorpet, Gränsö, and Berg; Fig. 2) were conducted for regional comparison.

3.2 Petrographical and textural analysis

Petrographical and textural analysis were conducted using a standard petrographical microscope. More detailed textural analysis and preliminary identification of minerals were performed during the electron microprobe sessions using back-scattered electron (BSE) imaging and energy-dispersive spectrometry analysis. This was performed on a JEOL JXA-8600 Superprobe at the University of Helsinki.

A CITL CL8200 Mk5-2 cold-cathode cathodoluminescence system coupled to a Leica DM2700 polarisation microscope and equipped with a Peltier-cooled Leica DFC450C high-resolution digital camera at the University of Helsinki was used for cathodoluminescence (CL) imaging of feldspars (Paper II) and apatite (Paper III). The beam current and voltage used were 0.25 mA and 7.0 kV, respectively.

3.3 Major and trace element mineral chemistry

Major and trace element analysis on REE-bearing minerals and gangue minerals were performed by electron-probe micro-analysis (EPMA) and laser-ablation inductively coupled plasma spectrometry (LA-ICP-MS) analysis at the University of Helsinki. EPMA was conducted on monazite-(Ce), xenotime-(Y), allanite-(Ce)–ferriallanite-(Ce), bastnäsite-(Ce) and synchysite-(Ce) (Paper I), on biotite, magnetite, amphibole (gedrite and anthophyllite), tourmaline (schorl-dravite and uvite), muscovite and chlorite (Paper II), and on fluorapatite (Paper III). All measurements were performed by wavelength-dispersive spectrometry on a JEOL JXA-8600 Superprobe integrated with the SAMx hardware and XMAs/IDFix/Diss5 analytical and imaging software package on carbon-coated thin or thick sections.

For the REE-bearing minerals, X-Ray lines were selected to minimise the interference between the different REE following the guidelines of Pyle et al. (2002). Beam current and accelerating voltage used were optimised and set to 25 nA and 20 kV, respectively. Analyses were performed with a defocused beam of ~7 μm diameter for monazite-(Ce) and xenotime-(Y), and a focused beam for allanite-(Ce)–ferriallanite-(Ce), bastnäsite-(Ce) and synchysite-(Ce). For biotite, magnetite, amphibole, tourmaline, muscovite and chlorite, all analyses were performed using a beam current of 15 nA, an accelerating voltage of 15 kV and a focused beam. For fluorapatite, the settings were optimised to minimise the F and Cl diffusion in apatite due to electron beam exposure (Stormer et al., 1993; Stock et al., 2015). Final conditions used were a defocused beam of ~15 μm, a beam current of 15 nA, and an accelerating voltage of 15 kV. Complete analytical details (X-Ray lines,

standards, counting times, and analyser crystals) can be found in Papers (I), (II) and (III), and their respective supplementary information.

LA-ICP-MS trace element analysis was performed with a Coherent GeoLas MV 193 nm laser-ablation system coupled to an Agilent 7900s ICP mass spectrometer. Trace element concentrations were measured in monazite-(Ce), xenotime-(Y), allanite-(Ce)–ferriallanite-(Ce) and bastnäsite-(Ce) (Paper I), in biotite and magnetite (Paper II), and in fluorapatite (Paper III). Flow rates were set to 15 L/min for Ar plasma gas, 1.0 L/min for He carrier gas, and 0.85 L/min for Ar auxiliary gas for during all sessions. Replicate measurements of the reference materials NIST SRM 610 and USGS GSE-1G were conducted to bracket the sample analyses and to correct for instrumental drift. NIST SRM 610 was selected as an external standard for monazite-(Ce), xenotime-(Y), bastnäsite-(Ce) and fluorapatite, whereas the GSE-1G standard was selected for biotite, magnetite, and allanite-(Ce)–ferriallanite-(Ce). For quantification of element concentrations, ^{27}Al (biotite and allanite-(Ce)–ferriallanite-(Ce)), ^{43}Ca (fluorapatite), ^{57}Fe (magnetite), ^{89}Y (xenotime-(Y)) and ^{140}Ce (monazite-(Ce) and bastnäsite-(Ce)) were selected as internal standards. Data treatment and quantification of LA-ICP-MS signals were done with the SILLS software package (Guillong et al., 2008).

Energy density, repetition rate and the number of pulses of the laser were optimised for the individual minerals. The accuracy of the LA-ICP-MS system has been verified and monitored by daily measurements of the reference material NIST SRM 612 as an unknown. The long-term accuracy for most elements is within 5% of the reference material (Spandler et al., 2011). Complete analytical details (laser settings, spot sizes, isotopes measured, dwell times) can be found in Papers (I), (II) and (III).

3.4 Stable Cl isotope and halogen analysis of fluorapatite

The in situ stable Cl isotopic and halogen (F, Cl, Br, and I) compositions of fluorapatite from the Olserum-Djupedal REE mineralisation were acquired by secondary ion mass spectroscopy (SIMS). These analyses were performed at the NORDSIM facility in Stockholm using a Cameca IMS1280 large geometry SIMS instrument. To avoid beam exposure to fluorapatite prior to analysis, the SIMS analyses were conducted on new epoxy mounts prepared from the same sample cut-offs as those used for the thin or thick sections, which were used during initial BSE imaging. These mounts were then gold-coated and pre-selected spots were measured with SIMS, one spot for the halogens and one for the Cl isotopes as close to each other as possible. EPMA and LA-ICP-MS analysis were subsequently performed on a spot adjacent to the SIMS spots.

The halogen and the Cl isotopic compositions were measured with a critically focused $^{133}Cs^{+}$ beam yielding a current of 1.2-1.6 nA for the halogen routine and 1.25-1.55 nA for the Cl isotopic routine. The mass resolving power was set to ~4000 M/ΔM for the halogens and ~2500 M/ΔM for the Cl isotopic routine. A field aperture of 3000 μm was used for both analytical routines to minimise surface contamination. The spots were also pre-sputtered for 90 s prior to analysis in a 20 by 20 μm area to reduce surface contamination. For the halogens, secondary ion intensities were collected over five scans with a total integration time of 120 s on Faraday cup (for species with counts > 10^6 cps) or electron multiplier (for species with counts < 10^6 cps). Because of the interference of CaCl species on ^{79}Br and ^{81}Br, Br was measured on the combined [$^{81}Br + {}^{44}Ca^{37}Cl + {}^{46}Ca^{35}Cl]^-$ mass peak. The peaks were normalised to the $^{40}Ca^{31}P$ matrix signal and the standard Durango apatite was used

to determine absolute concentrations. Measurements of the Durango standard (n = 25) yielded a relative standard deviation of 1% for F, 1.2% for Cl, 11.4% for Br, and 1.5% for I. For the Cl isotopic analysis, ^{35}Cl and ^{37}Cl were collected simultaneously using multicollection mode on Faraday cup with an overall counting time of 160 s, conducted over four blocks of ten integrations. Measurements of the Durango apatite standard with a known isotopic composition ($\delta^{37}Cl$ = +0.5‰) were regularly interspersed between the unknowns to correct for instrumental drift and matrix-dependent instrumental fractionation. The Cl isotopic compositions are expressed using the δ-notation defined as:

$$\delta^{37}Cl\ (‰) = \{[(^{37}Cl/^{35}Cl)_{sample} - (^{37}Cl/^{35}Cl)_{SMOC}] / (^{37}Cl/^{35}Cl)_{SMOC}\} \cdot 1000$$

where SMOC is the Standard Mean Ocean Chloride with a defined value of 0.0‰ (Kaufmann et al., 1984). The reproducibility of $\delta^{37}Cl$ was 0.09 to 0.20‰ based on multiple measurements (n = 50) of the Durango apatite standard during three analytical sessions.

3.5 Fluid inclusion microthermometry and LA-ICP-MS analysis

Fluid inclusions were studied on double-polished thick sections of quartz (200 to 500 μm thickness). Microthermometry was performed on a Linkam THMSG-600 heating-freezing stage mounted on a Leica DM2500P petrographic microscope. Daily calibration was made using synthetic H_2O, H_2O-NaCl and H_2O-CO_2 fluid inclusion standards (SynFlinc™). Calibration was performed against the H_2O-CO_2 Q3 quadruple point (–56.6 °C), the H_2O-NaCl eutectic (–21.2 °C), and the melting of ice (0.0 °C). Heating runs were calibrated against the critical temperature of H_2O (374.1 °C). Estimated reproducibility for freezing experiments is 0.3 °C and that for heating runs is c. 5 °C.

For L-V inclusion, salinity was calculated from the final ice melting temperature assuming NaCl-H_2O compositions using the equation of Bodnar (1993). For L-V-S inclusions, three different types were recognised based on appearance at room temperature, behaviour during microthermometry and compositions determined by LA-ICP-MS. Different approaches were used to estimate the salinities of these fluid inclusions depending on the type. For L-V-S inclusions approximated by the NaCl-$FeCl_2$-KCl-$CaCl_2$-H_2O system (Na-Fe-K-Ca brines; Table A1), an estimated total salinity of 45 wt% for all fluid inclusions assemblages (FIA) was used based on an average temperature of halite melting of 300 °C. L-V-S inclusions in the $CaCl_2$-NaCl-H_2O system (Ca-Na brines) did not freeze during cooling, and melting of ice, hydrohalite or antarcticite could not be observed. Salinity and bulk composition were thus estimated by combining the measured mass Na/(Na+Ca) ratio by fluid inclusion LA-ICP-MS analysis and the temperature of halite melting (final melting temperature; Steele-MacInnis et al., 2011). Halite melting temperatures were initially measured for many of the FIA's after LA-ICP-MS analysis to avoid the risk of decrepitation of fluid inclusions during heating prior to LA-ICP-MS analysis (marked with * in Table A1). However, because of the low halite melting temperatures of these inclusions (< 200 °C), halite melting temperatures could be measured prior to LA-ICP-MS analysis for the FIA's targeted during the second session of LA-ICP-MS analysis. An average Na/(Na+Ca) ratio (of 0.125) was used for the FIA's not analysed by LA-ICP-MS. For one FIA (sample EJ-14-2B, FIA17), melting of antarcticite was observed. The salinity and bulk composition could thus be calculated using melting temperatures of antarcticite and halite, which yield a similar Na/(Na+Ca) ratio and salinity as those calculated

using this ratio determined by LA-ICP-MS analysis and halite melting temperatures. For L-V-S inclusions in the NaCl-$CaCl_2$-(KCl)-H_2O system (Na-Ca brines), salinity and bulk composition were calculated using the ice and halite melting temperature employing the graphical method of Vanko et al. (1988).

Fluid inclusion LA-ICP-MS was performed using an Agilent 7900s quadrupole ICPMS coupled to a Coherent Geolas Pro MV 193 nm excimer laser-ablation system at the University of Helsinki. A 1 cm^3 ablation cell was used for fast washout to ensure high element sensitivities and low limits of detections. The analytical protocol and settings used followed that of Fusswinkel et al. (2017, 2018). Elements measured were ^{7}Li, ^{11}B, ^{23}Na, ^{24}Mg, ^{27}Al, ^{39}K, ^{44}Ca, ^{49}Ti, ^{55}Mn, ^{56}Fe or ^{57}Fe, ^{66}Zn, ^{85}Rb, ^{88}Sr, ^{133}Cs, ^{137}Ba, ^{208}Pb, ^{89}Y, ^{140}Ce, ^{146}Nd, ^{35}Cl, ^{81}Br, and ^{127}I. Data treatment was performed with the SILLS software package (Guillong et al., 2008). Elements were quantified using the reference material NIST SRM 611 as an external standard, except for Cl, Br, and I. The halogens were standardised to the natural scapolite standard Sca-17 (Seo et al., 2011; Fusswinkel et al., 2018). Concentrations were calculated using Na concentrations (as NaCl equivalent) determined from microthermometry as an internal standard. A mass balance routine implemented in the SILLS software using cation/chlorine ratios from the LA-ICP-MS signals was used to determine the bulk fluid composition. Cations used for mass balancing were Na, Ca, K, or Fe depending on the fluid inclusion type. The intervals for the fluid inclusions were selected based on the peaks of the major components in the fluid inclusions (Ca, Na, and Cl) and the return of these signals to the background level. The signals of all remaining elements were carefully checked for each of the fluid inclusions. Calculated element concentrations for the remaining elements were rejected if the signals were not synchronous with the major element signals. Host correction was made assuming 100% SiO_2 and by closely bracketing the fluid inclusions signals. Fluid inclusion LA-ICP-MS data are presented as FIA averages (Table A2).

4 Summary of original papers

4.1 Paper I. Mineralogy, paragenesis, and mineral chemistry of REEs in the Olserum-Djupedal REE-phosphate mineralization, SE Sweden

This study established the mineralogical, textural and mineral-chemical framework for a relatively unusual hydrothermal REE mineralisation in the Olserum-Djupedal district in SE Sweden. By combining mineralogical and petrological studies with mineral chemistry of the REE mineral phases, we could show that abundant xenotime-(Y) and monazite-(Ce) co-crystallised with fluorapatite and subordinate (Y,REE,U,Fe)-(Nb,Ta)-oxides during an initial high-temperature stage (~600-650 °C). These mainly formed within veins dominated by biotite, magnetite, amphibole, and quartz. Further, following the evolution of the hydrothermal fluid, allanite-(Ce) formed locally. Subsequent cooling of the hydrothermal system induced alteration and replacement of primary xenotime-(Y), monazite-(Ce), fluorapatite and (Y,REE,U,Fe)-(Nb,Ta)-oxides, which resulted in the remobilisation of REE, Th, U and Nb-Ta, and the formation of secondary monazite-(Ce), xenotime-(Y), fluorapatite and allanite-(Ce)–ferriallanite-(Ce) and subordinate uraninite, thorite, columbite-(Fe) and (Th,U,Y,Ca)-silicates. Monazite-xenotime thermometry showed that these alteration processes occurred down to temperatures of about ~400 °C. Bastnäsite-(Ce) and

minor synchysite-(Ce) formed from lower-temperature (<400 °C) alteration of allanite-(Ce) and allanite-(Ce)–ferriallanite-(Ce) and represented the latest stage of REE mineral formation. The mineralogy and alteration processes between the two main mineralisation areas, i.e., Olserum and Djupedal areas, were found to differ from each other slightly. This was interpreted to result from the increase in the Ca concentration of the fluid in the Djupedal area. This caused the formation of allanite-(Ce) and extensive replacement of primary monazite-(Ce). This contrasts with the REE assemblages in the Olserum area, where no allanite-(Ce) formed and monazite-(Ce) only exhibited moderate replacement to secondary fluorapatite. The primary hydrothermal REE-bearing assemblages and alteration processes in the Olserum-Djupedal mineralisation demonstrate the joint mobility of REE, Th, U, and Nb-Ta in F-bearing high-temperature fluids.

4.2 Paper II. Origin of the high-temperature Olserum-Djupedal REE-phosphate mineralisation, SE Sweden: A unique contact metamorphic-hydrothermal system

This study combined field and petrographic relationships with major and trace element chemistry of the main gangue minerals to constrain the timing and origin of the Olserum-Djupedal REE mineralisation. Field relationships revealed that REE mineralisation is exposed at three main areas; Olserum, Bersummen and Djupedal, and dominantly occurs as ESE-WNW to SE-NW trending veins and vein zones in metasedimentary rocks in or close to the contact aureole of a ferroan, peraluminous alkali-feldspar granitic pluton. The veins and vein zones host abundant monazite-(Ce), xenotime-(Y) and fluorapatite, which are variably fractured and recrystallised. REE-bearing veins were also found to be hosted within a granite to granitic gneiss present in the outermost parts of the pluton. The veins and vein zones are frequently transected by abundant pegmatitic to granitic dykes in Olserum and Bersummen areas. In the Djupedal area, extensive post-mineralisation migmatisation formed within the REE-mineralised metasedimentary rocks. Collectively, the field evidence led us to suggest a close association of the REE mineralisation with the granite.

The major and trace element chemistry of co-existing biotite and magnetite revealed that all the mineralised areas belong to the same REE-mineralising system. High concentrations of Na in biotite and amphibole and the abundance of biotite indicated a Na-K-rich character of the original REE-mineralising fluid forming the REE-phosphates. As shown by the presence of Ca-rich minerals such as allanite-(Ce) and calcic tourmaline (uvite) in the Djupedal area, the fluid evolved to more Na-Ca-rich compositions during cooling of the hydrothermal system. At this stage, alteration of the granite and the wall rocks induced by the Ca-Na nature of the fluids produced distinct white quartz-plagioclase rocks. Halogen fugacities as calculated from biotite compositions showed that the primary REE-mineralising fluid was Cl-dominant, but with a high F component. The calculated log(fHF/fHCl) values decrease in a sequence from granite- and metasediment-hosted biotite in the Olserum area ($\log(f_{HF}/f_{HCl})$ of –1.0 to –1.2) to metasediment-hosted biotite in the Bersummen ($\log(f_{HF}/f_{HCl})$ of –1.5 to –1.8) and Djupedal areas ($\log(f_{HF}/f_{HCl})$ of –1.6 to –2.0).

The combined evidence led us to propose a hydrothermal origin of the REE mineralisation, formed by granitic-derived REE-P-Cl-F-enriched fluids expelled at an early stage of the magmatic evolution. Following this, an older model involving the assimilation and remobilisation of former heavy mineral-rich beds was discarded. The primary REE mineralisation and

alteration processes in the Olserum-Djupedal district were probably coeval with regional-scale K-Na and Na-Ca metasomatism closely associated with granitic magmatism at around 1.8 Ga in the Västervik region.

4.3. Paper III. Apatite as a tracer of the source, chemistry, and evolution of ore-forming fluids: the case of the Olserum-Djupedal REE mineralisation, SE Sweden.

This study explored the suitability of using apatite as a tracer of the source, chemistry, and evolution of ore-forming fluids using the halogen (F, Cl, Br, and I), stable Cl isotopic and trace element compositions of fluorapatite from the Olserum-Djupedal REE mineralisation in SE Sweden. Based on the textural relations and mineral-chemical compositions, four main fluid events were recognised; 1) deposit-scale zoning of primary fluorapatite representing the primary hydrothermal fluid flow, 2) high-temperature dissolution-reprecipitation processes following primary fluorapatite formation, 3) internal zoning of primary fluorapatite caused by lower-temperature remobilisation, and 4) secondary fluorapatite replacing primary monazite-(Ce). The primary hydrothermal fluid flow was recognised as a down-temperature flow and was recorded in a sequence from granite-hosted fluorapatite, via metasediment-hosted fluorapatite in the Olserum area to metasediment-hosted fluorapatite in the Bersummen and Djupedal areas. This sequence recorded a gradual increase in Cl (~800 to 5000 ppm) and Br (~1 to 20 ppm) concentrations, and a decrease of F (~3.75 to 2.9 wt%) and I (~0.75 to 0.45 ppm) concentrations and in $\delta^{37}Cl$ values (+1.0 to –0.5 ‰). Calculated $\log(f_{HF}/f_{HCl})$ values of primary fluorapatite followed those of co-existing biotite for the defined sequence, indicating that the incorporation of the halogens into apatite are dominantly governed by the chemistry of the evolving ore-forming fluid. Later low-temperature remobilisation was found to only cause marginal changes in halogen and trace element concentrations in specific domains of the fluorapatite crystals (rims, recrystallised grains, and domains adjacent to fractures), whereas $\delta^{37}Cl$ values remained unchanged. This suggests that apatite can retain its initial composition inherited by the original ore-forming fluid despite later overprinting fluid events.

As apatite was found to be sensitive to changing fluid compositions, apatite showing the chemically least evolved character needed to be recognised in order to trace the origin of the primary ore-forming fluid. In the Olserum-Djupedal REE mineralisation, this corresponds to the granite-hosted primary fluorapatite. This fluorapatite has $\delta^{37}Cl$ values (–0.4 to +1.6 ‰) and molar halogen ratios (Br/Cl of 0.45 to 0.80 $\cdot 10^{-3}$ and I/Cl of 190 to 310 $\cdot 10^{-6}$) comparable to fluids associated with S-type granites in SE England ($\delta^{37}Cl$ of +1.7 to +2.0 ‰, Br/Cl of 0.45 to 0.9 $\cdot 10^{-3}$ and I/Cl of 50 to 110 $\cdot 10^{-6}$), which have a similar petrogenesis as the Olserum-Djupedal granite. The small fractionation of Br from I observed between altered fluorapatite and Na-Ca and Ca-Na fluid inclusions analysed by LA-ICP-MS suggested that Br and I do not necessarily fractionate to the degree proposed earlier and that Br and I may even have comparable partition coefficients ($D^{Br}_{apatite\text{-}fluid}$ and $D^{I}_{apatite\text{-}fluid}$). This led us to interpret the halogen signatures and the stable Cl isotopic composition of the granite-hosted fluorapatite to represent an original magmatic fluid.

No trace element in primary fluorapatite adhered to the trend defined by the deposit-scale zoning. This suggested that trace element compositions of apatite are mostly influenced by host rock environment and co-crystallisation with other minerals. However, the characteristically elevated Fe concentrations of primary

fluorapatite may suggest elevated $FeCl_2$ of the ore-forming fluid. Moreover, the REE and particularly normalised ratios (La/Sm, La/Yb, Gd/Yb, and Y/Ho) were found to trace the evolution of the primary ore-forming fluid and can also discriminate between apatite forming by mineral replacement from apatite forming from the primary ore-forming fluid. In conclusion, apatite was found to be suitable in tracing the source, chemistry, and evolution of ore-forming fluids.

5 Discussion

5.1 Textural, mineralogical and fluid-chemical evolution of the hydrothermal Olserum-Djupedal REE-phosphate mineralisation

This section aims to bring together the early four-stage paragenesis model (Paper I) with new findings from subsequent papers and from fluid inclusion data into a new integrated model (Fig. 4). During stage A, primary mineralisation started at high temperatures (550-650 °C) with the formation of coeval fluorapatite, monazite-(Ce) and xenotime-(Y) with subordinate (Y,REE,U,Fe)-(Nb,Ta)-oxides. These formed in veins and vein zones dominated by biotite-magnetite from fluids exsolved from the Olserum-Djupedal granite early during crystallisation and fractionation. The veins and vein systems developed primarily in metasedimentary rocks in the contact aureole of the granite and within the outermost zone of the granite. Primary mineralisation took place at c. 1.8 Ga, coeval with the crystallisation of Olserum-Djupedal granite. Fluid flow was presumably from the granite towards the metasedimentary rocks, with the mineralisations in the Bersummen and Djupedal areas forming in a more distal position.

No fluid inclusions from the primary ore-forming stage have been identified. In paper II and III, biotite and fluorapatite have been used as proxies for the ore-forming fluid. Halogen compositions of biotite and fluorapatite indicate that the REE-mineralising fluid was at first dominantly Cl-bearing but with a relatively high F concentration. Subsequent crystallising of fluorapatite and biotite depleted the fluid in F, passively enriching the fluid in Cl. The relatively high F concentration in the fluid aided with the transport of high field strength elements (HFSE) such as Nb-Ta and Th that accompanied the REE in the primary REE-mineralising fluid (e.g., Keppler and Wyllie, 1990, 1991; Jiang et al., 2005; Timofeev et al., 2015, 2017).

The mineral paragenesis and major and trace element chemistry of the main gangue minerals suggest a Na-K-Fe-Ca dominated composition of the primary ore-forming fluid. Initially, the fluid probably possessed a high K/Na ratio because of the abundance of biotite precipitated from this fluid. The Ca concentration must have been relatively high too to precipitate fluorapatite but low enough to promote the formation of REE-phosphates from the available P in the fluid instead of only fluorapatite. In addition, the Ca and F concentrations were sufficiently low to inhibit fluorite saturation. L-V-S fluid inclusions identified in quartz from pegmatitic dykes cross-cutting the REE ore in the Olserum area exhibit Na-Fe-K-Ca compositions (Table A2). Although these inclusions likely represent a more evolved and trapped fluid, as indicated by low homogenisation temperatures and by the occurrence in cross-cutting pegmatite dykes, they are likely close in composition to the original REE-mineralising fluid.

Incipient dissolution and re-precipitation of fluorapatite forming monazite-(Ce) and xenotime-(Y) inclusions took place when the hydrothermal system was still at high temperatures, comparable to those forming the primary min-

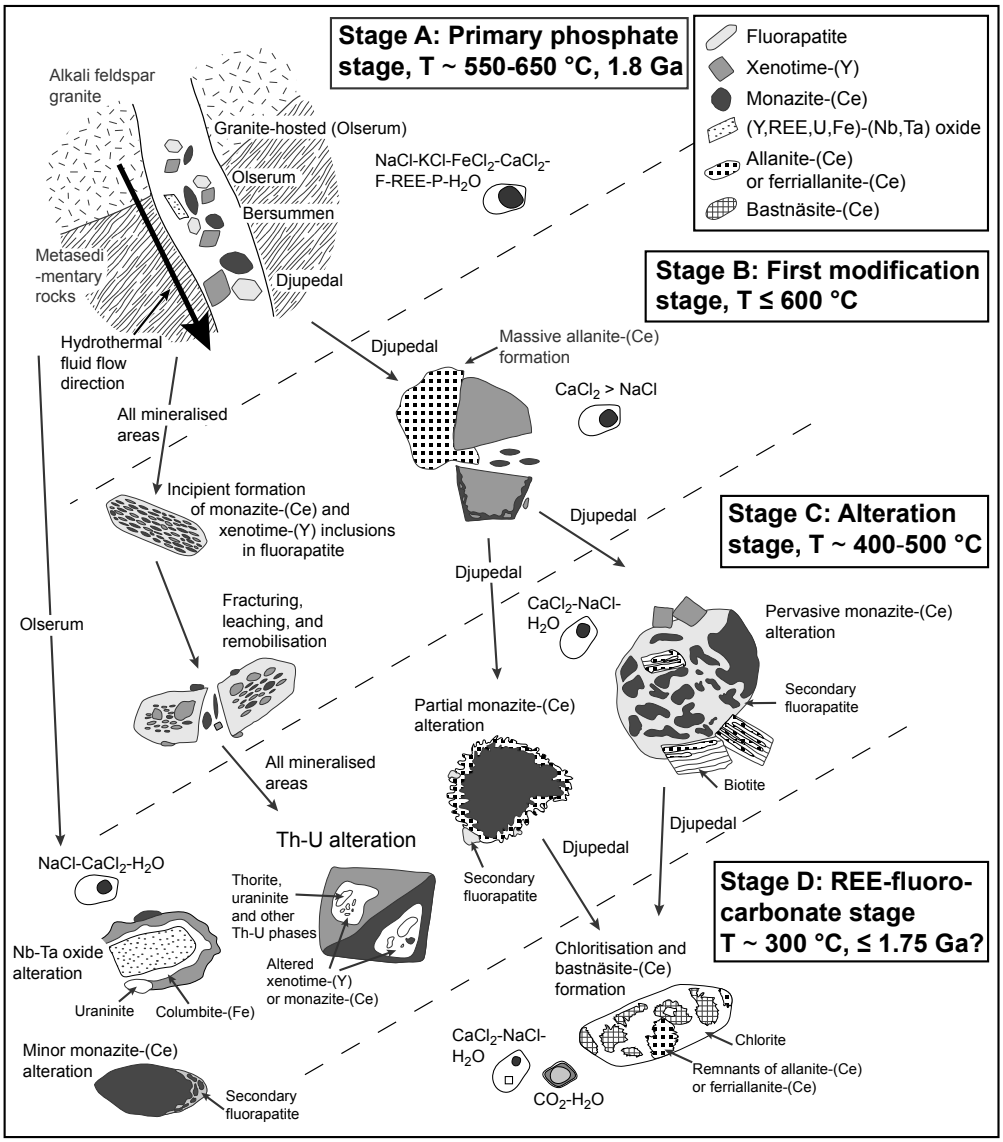

Fig. 4. A modified schematic illustration showing the textural evolution of the REE-mineralising system in the Olserum-Djupedal REE mineralisation. Modified after Paper I.

eralisation. The fracturing of primary minerals during stage B aided in the modification of the primary ore assemblages by initiating remobilisation of REE and other elements. In the Djupedal area, the fluid evolved to more calcic compositions, promoting the formation of allanite-(Ce) and calcic tourmaline (uvite).

During subsequent cooling, the ore assemblages were further modified during stage C by extensive alteration, which caused remobilisation of REE, Th, U, and Nb-Ta. Highly calcic fluids in the Djupedal area triggered the pervasive and partial alteration of monazite-(Ce) forming secondary fluorapatite and allanite-(Ce)–ferriallanite-(Ce). The calcic fluids also promoted the formation of accessory fluorite and scheelite. In the Olserum and Bersummen areas, monazite-(Ce) only exhibits moderate re-

placement to secondary fluorapatite indicating a lower calcic component of the metasomatic fluid. Monazite-(Ce) and xenotime-(Y) from all mineralised areas were heavily altered, resulting in the formation of uraninite, thorite and other (Th,U,Y,Ca)-silicates. Local alteration of primary (Y,REE,U,Fe)-(Nb,Ta)-oxides led to the formation of columbite-(Fe), uraninite, xenotime-(Y) ± monazite-(Ce). Monazite-xenotime thermometry showed that these alteration processes occurred down to temperatures of about ~400 °C.

The clear difference in alteration assemblages between the Olserum and Bersummen areas to that of the Djupedal area were caused by chemically distinct fluids. High-density L-V-S fluid inclusions have been found in quartz from the Djupedal area (Ca-Na brines; Table A1 and A2) and in quartz from the Olserum area (Na-Ca brines). Although they were trapped at lower temperatures (probably below 300 °C) than the inferred lower-temperature limit for this alteration stage, they show distinct chemical compositions that likely depict the differences in fluid compositions between the areas during the alteration stage. High-density fluid inclusions in the Djupedal are very calcic, whereas similar high-density fluid inclusions in the Olserum area are more sodic but still relatively rich in Ca (Table A2). Such a difference in composition is consistent with the alteration features recognised in the different mineralised areas.

The formation of bastnäsite-(Ce) marks the latest stage of REE-mineral formation. Bastnäsite-(Ce) formed locally in the Djupedal area during chloritisation of allanite-(Ce) or allanite-(Ce)–ferriallanite-(Ce). This required CO_2-rich fluids. Quartz from the Djupedal area frequently contains secondary fluid inclusion arrays with almost pure low-density CO_2 inclusions (Table A1). The Ca-Na brine inclusions from the Djupedal area also frequently co-exist with similar CO_2 inclusions. The Ca-Na brine inclusions also contain a carbonate solid phase and rarely hematite. Halogen (Cl, Br, and I) measurements of the brine inclusions show that they are very rich in Br and I relative to seawater (Fig. 5). The very high salinity and the high Br/Cl and I/Cl ratios are proposed to result from fluid desiccation during the chloritisation of biotite, allanite-(Ce) or allanite-(Ce)–ferriallanite-(Ce) and, in part, magnetite, where chlorite sequestered H_2O from the fluid. This also resulted in halite precipitation, which can explain the increasing Br and I in the fluid as they are both incompatible in halite (Holser, 1979; Campbell et al., 1995; Fusswinkel et al., 2018). Because bastnäsite-(Ce) formed during the chloritisation of allanite-(Ce) or allanite-(Ce)–ferriallanite-(Ce), it is likely that the Ca-Na brine was related to this and trapped in quartz after bastnäsite-(Ce) had formed. Low trapping temperatures of the Ca brine inclusions (< 300 °C) indicate that bastnäsite-(Ce) formed at around 300 °C. Alteration of the primary mineralisation stage likely occurred to at least 1.75 Ga.

Some primary fluorapatites in the Olserum area have distinctly different Br/Cl and I/Cl signatures following the fluid desiccation trend (Fig. 5). Hematite trapped in the Ca-Na brine inclusions demonstrates that hematite was stable during the entrapment of the Ca-Na and Na-Ca brines. Hematite is extensively replacing magnetite in the surrounding mineral matrix of this type of fluorapatite. It is thus likely that the halogen chemistry of this fluorapatite was inherited by alteration fluids similar to the Na-Ca and Ca-Na brines when extensive martitisation took place. I have also observed a more intense martitisation of magnetite in the Djupedal area where quartz contain abundant Na-Ca fluid inclusions. The good agreement between this fluorapatite and the measured fluid inclusions indicates a smaller fractionation of Br from I during apatite precipitation.

By using the halogen compositions of the

granite-hosted fluorapatite, the primary hydrothermal fluid composition can be calculated. This calculation is based on the partition coefficients for Br and I between apatite and fluid ($D^{Br}_{apatite-fluid}$ ~0.005-0.009 and $D^{I}_{apatite-fluid}$ ~0.007-0.013), derived from the halogen compositions of the altered fluorapatite and the fluid inclusions, and an estimation of the fluid salinity. The resulting halogen composition of the primary hydrothermal fluid for a reasonable salinity of 10 wt% NaCl eq., equals to molar Br/Cl and I/Cl ratios of ~$1.1 \cdot 10^{-3}$ and $350 \cdot 10^{-6}$, respectively (Fig. 5). Such a fluid composition is plausible for a magmatic-hydrothermal fluid related to S-type magmatism. The elevated I/Cl ratio could reflect a source of the granitic melts in the Olserum-Djupedal district enriched in I relative to the granites defining the S-type field.

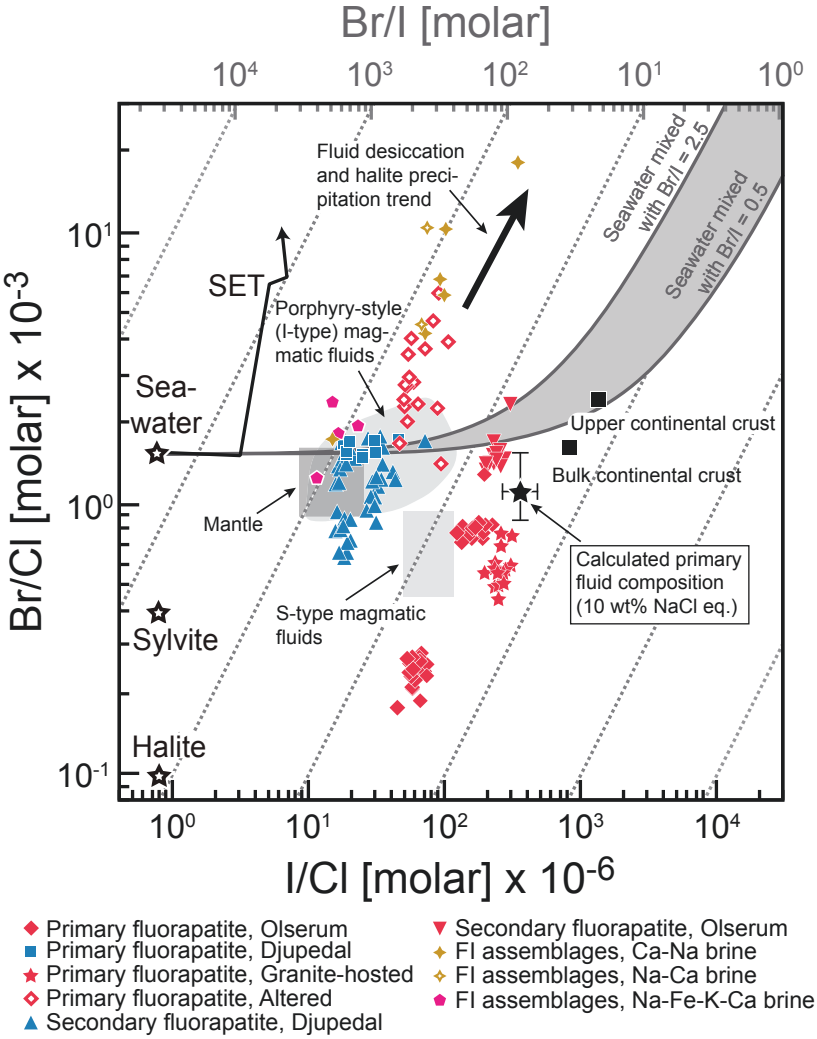

Fig. 5. Diagram of the molar Br/Cl ratio versus the I/Cl ratio for data of the Olserum-Djupedal REE-phosphate mineralisation. The porphyry-type magmatic field is defined by data from Irwin and Roedder (1995), Kendrick et al. (2001) and Seo et al. (2011) and the S-type magmatic fluid field by data from Böhlke and Irwin (1992), Irwin and Roedder (1995), Banks et al. (2000a, 2000b), and Seo et al. (2011). The mantle field is defined by data from Kendrick et al. (2013, 2017). The average values for the bulk continental crust and upper continental crust are adopted from Rudnick and Gao (2003). SET is the seawater evaporation trend. Diagram modified after Fusswinkel et al. (2018).

In summary, primary REE mineralisation formed from granitic-derived fluids at high temperatures (~600 °C) at c. 1.8 Ga. The fluids were relatively reducing and dominated by Na-K-(Fe-Ca)-Cl-F, which locally evolved to more Cl- and Ca-bearing fluids. During subsequent cooling of the hydrothermal system, the ore assemblages were variably altered by Ca-Na to Na-Ca-dominated fluids down to temperatures of around 300 °C to at least 1.75 Ga.

5.2 Source of REE and P in REE-phosphate deposits

Because many hydrothermal REE-phosphate deposits are associated with alkaline magmatic rocks, particularly carbonatites, it is warranted to discuss first what type of processes enrich the REE and, in part P, in carbonatites. Because carbonatites commonly co-exist with coeval ultramafic and alkaline rocks, their origin have mainly been assigned to fractional crystallisation or liquid immiscibility of alkali-rich carbonatite-silicate magmas derived from the lithospheric or asthenospheric mantle, whereas only a few may originate directly from low-degree mantle melts (Mitchell, 2005; Chakhmouradian and Zaitsev, 2012).

The endowment of REE in carbonatites can be explained either by fractional crystallisation of REE-poor oxides and silicate minerals and subsequent extraction of a carbonatite fractionated melt, or by carbonatite-silicate liquid immiscibility because the REE (and P) mostly prefer the carbonatite melt over the silicate melt (Chakhmouradian and Zaitsev, 2012; Veksler et al., 2012; Martin et al., 2013). Because apatite solubility is high in carbonatite melts compared to silicate melts (Watson and Capobianco; 1981; Harrison and Watson, 1984; Wolf and London, 1994; Hammouda et al., 2010; Chakhmouradian et al., 2017), fractional crystallisation in a pure carbonatite system will lead to an enriched P concentration in the melt. In carbonatite-silicate systems, however, specific rocks with very high P_2O_5 contents, usually termed phoscorite occur (Chakhmouradian et al., 2017, and references therein). Other parameters than apatite solubility, such as the activity of F and P, and possible fluid exsolution, thus dictate whether apatite will crystallise as a cumulate phase or if P will be enriched in a residual carbonatite melt. Because the REE are compatible in apatite, REE will be depleted in carbonatite-silicate systems where significant apatite fractionation occurs, although fractionation of other minerals and magma replenishment also affects the REE budget in such systems (Chakhmouradian et al., 2017). Yet, carbonatites or carbonatite-alkaline silicate systems exhibit strong affinities for REE, especially LREE (Fig. 6), and for P. The observation that monazite, which typically forms by late hydrothermal-carbothermal processes (e.g., Zaitsev et al., 2015; Chakhmouradian et al., 2017, and references therein; Marien et al., 2018), is the principal REE-mineral in many hydrothermal REE deposits associated with carbonatites is thus not surprising considering the high probability for mobilisation of REE and P in such systems.

In peralkaline quartz-saturated rocks that exhibit a strong affinity for the REE (Fig. 6), the P content is usually low (e.g., Boily and Williams-Jones, 1994; Dostal et al., 2014, Möller and Williams-Jones, 2016), presumably due to early fractionation of apatite as result of the low solubility of apatite in peralkaline silicate magmas (Watson and Capobianco, 1981). In quartz-undersaturated peralkaline systems, which also are strongly affiliated with high REE concentrations (Fig. 6), the P concentration can be high too, especially in cumulate units related to alkaline-carbonatite magmatism (e.g., rocks in the Kola Province; Zaitsev et al., 2015, and references therein). However, mona-

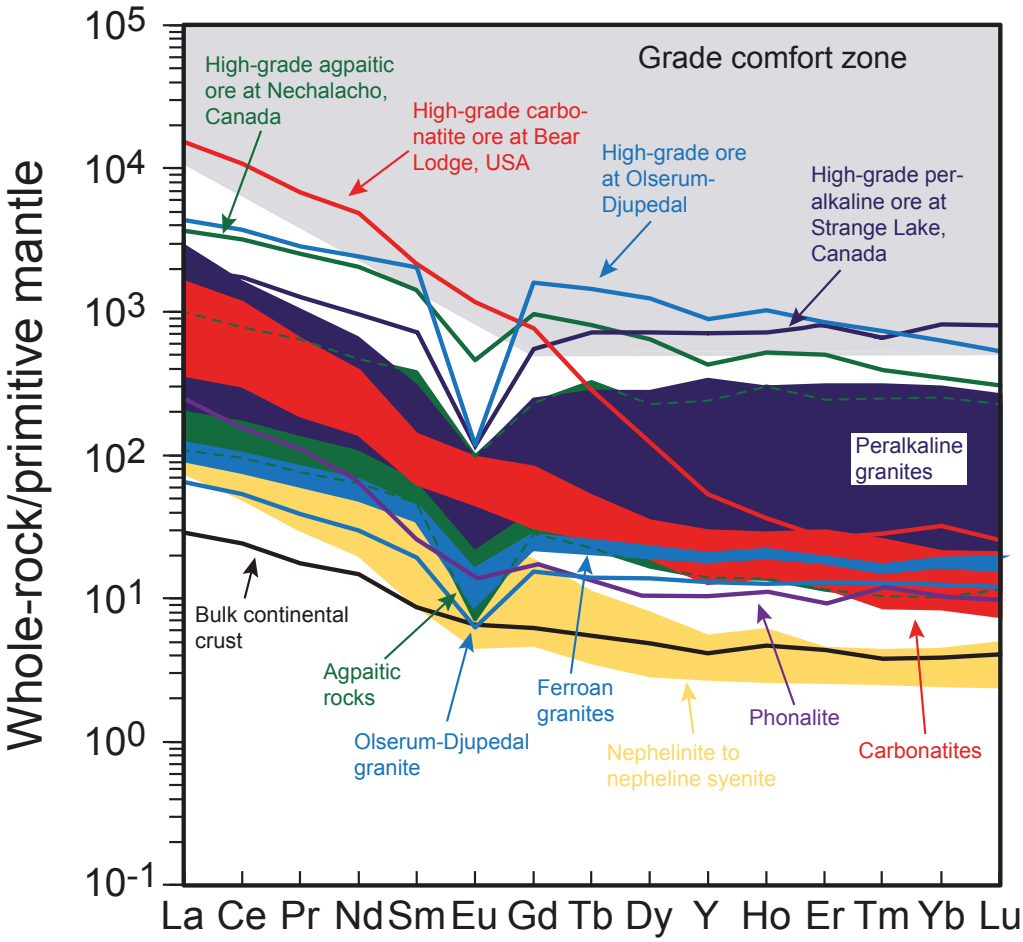

Fig. 6. Whole-rock REE distribution diagrams normalised to primitive mantle for the most relevant magmatic sources of REE. Modified after Chakmouradian and Zaitsev (2012). Normalisation after McDonough and Sun (1995). Note that the field of nephelinite to nepheline syenite continues under the fields of the agpaitic and peralkaline rocks on the LREE-side of the diagram and that the agpaitic field overlaps with the peralkaline granites (indicated by dashed green lines). Sources: peralkaline granites (Boily and Williams-Jones, 1994; Kovalenko et al., 1995; Kynicky et al., 2011; Dostal et al., 2014; Möller and Williams-Jones, 2016); agpaitic rocks (Sørensen et al., 2006; Sjöqvist et al., 2013; Möller and Williams-Jones, 2016); carbonatites (Lottermoser, 1990; Xu et al., 2008; Moore et al., 2015; Trofanenko et al., 2016; Bodeving et al., 2017; Marien et al., 2018); bulk continental crust (Rudnick and Gao, 2003); ferroan granites (Collins et al., 1982); the others are from Chakmouradian and Zaitsev (2012).

zite or xenotime are uncommon hydrothermal minerals associated with such rocks.

For the REE-phosphate rich Olserum-Djupedal REE deposits, no alkaline source of REE is plausible because of the complete lack of rocks with such compositions with the same age (1.8 Ga) in the Västervik region. Alkaline rocks of Palaeoproterzoic age in the Fennoscandian Shield mainly occur in Finland, including the c. 1830 Ma Korsnäs carbonatite (Sarapää et al., 2013), the c. 1792 Ma Halpanen carbonatite (Rukhlov and Bell, 2010) and the c. 1796 Ma Naantali carbonatite (Woodard and Hetherington, 2014). The Almunge syenite complex in Bergslagen is the closest alkaline rocks with a similar age in Sweden (c. 1.88 Ga; Delin and Bastani, 2009). Peralkaline agpaitic rocks at the Norra Kärr alkaline complex are geographically close but are much younger (1.49 Ga; Sjöqvist et al, 2017). The Naantali carbonatite

dykes intruded at a similar age as that inferred for the Olserum-Djupedal REE mineralisation, suggesting that carbonatites may have formed at depth during the tectonic regime that was prevalent at that time (cf., Rutanen et al., 2011; Woodard and Hetherington, 2014). However, several lines of evidence strongly suggest a granitic source of the REE for the Olserum-Djupedal REE mineralisation: 1) field relationships indicate a strong spatial and temporal relationship of the mineralisation with the dominant TIB Olserum-Djupedal granite in the district (Fig. 3), 2) the halogen compositions of fluorapatite indicate a hydrothermal fluid flow from this granite towards the metasedimentary host rocks and, 3) the halogen and Cl isotopic compositions of fluorapatite is consistent with a granitic source of the ore-forming fluids. In addition, the composition of the Naantali carbonatite is LREE-dominated (Woodard and Hetherington, 2014), whereas the ore at Olserum-Djupedal REE mineralisation is more HREE-rich (Fig. 6). The mineral-chemical compositions of fluorapatite and monazite-(Ce) from the Olserum-Djupedal REE mineralisation are also distinct from those of the Naantali carbonatite (Woodard and Hetherington, 2014).

Findings from this study suggest that REE and P can be derived from other sources than alkaline magmatic sources. The clear association of the Olserum-Djupedal REE mineralisation with the peraluminous Olserum-Djupedal granite suggests that REE and P were derived from this magmatic system. But how can the high-grade REE-phosphate ore (Fig. 6) be reconciled with the generally low REE ($\sum$REE ~300 ppm) and P (0.04-0.07 wt% P_2O_5) contents of the granite?

The solubility of apatite in silicate rocks is highest for hot mafic melts compared to colder felsic melts. In metaluminous silicate melts, the P_2O_5 concentration decreases with increasing fractionation towards high silica members as a result of decreasing temperature and solubility of apatite (Watson, 1979, 1980; Watson and Capiobianco, 1981; Harrison and Watson, 1984; Piccoli and Candela, 2002). In peraluminous silicate melts, the solubility of apatite increases with peraluminousity, and peraluminous granites can have significantly higher P_2O_5 contents than metaluminous granites with similar silica contents (Bea et al., 1992, 1994; Pichavant et al., 1992; Wolf and London, 1994). The solubilities of monazite and xenotime are low and decrease with increasing peraluminosity, and are highest for peralkaline silicate melts (Montel, 1986, 1993; Rapp et al., 1987; Wolf and London, 1995). Thus, for peraluminous melts, melting at the source will generate a melt undersaturated in apatite and crystallisation of feldspar will increase the P/Ca ratio so that excess P can be incorporated into P-minerals with low solubilities such as monazite or xenotime and into K-feldspars with increasing fractionation and peraluminosity (London et al., 1999; Piccoli and Candela, 2002). This is consistent with the Olserum-Djupedal granite, which contains xenotime-(Y) and monazite-(Ce) but rarely primary fluorapatite. Xenotime-(Y) and monazite-(Ce) are predominantly enriched in biotite-magnetite schlieren in the granite and rarely as disseminated grains within the groundmass. London (1992) noted that P exhibits highly nonideal mixing in felsic melts, which can cause local heterogeneities due to unmixing of P-enriched domains. Local high P solubility can probably also stem from local heat fluxes. Notably, London (1992) further suggested that these P-enriched domains would accumulate with REE and other HFSE in basic and Fe-rich melts domain. This could explain the common and local occurrence of monazite-(Ce) and xenotime-(Y), and zircon within the biotite-magnetite schlieren. Thus, the low REE and P whole-rock contents may not necessarily imply low REE and

P concentrations of the original melt. In addition, P can be lost to pegmatites formed from more evolved P-enriched residual melts via filter-pressing or be lost due to extensive sericitic and argillic alteration of alkali feldspars (London, 1992; London et al., 1993).

Although the Olserum-Djupedal granitic system yet is poorly understood, abundant pegmatitic and granitic dykes and veins crosscut both the main granitic body and the surrounding ore-bearing metasedimentary rocks. These dykes and veins contain sillimanite, which indicates a strongly peraluminous character, and the dykes and veins probably represent the most evolved melt. Primary fluorapatite is rare in these dykes and veins too, but fine-grained secondary fluorapatite is abundant close to or in altered feldspar domains. This could imply that feldspar in these evolved rocks initially contained high P concentrations, which were released and formed fluorapatite during feldspar alteration. It is thus quite plausible that P to some extent was extracted from the initial melt and enriched in P-rich pegmatites.

Fluid exsolution could also sequester REE and P from the melt. The REE almost invariably partition in favour of the melt over the fluid/vapour (London et al., 1988; Webster et al., 1989; Reed et al., 2000; Zajacz et al., 2008; Borchert et al., 2010). However, partition coefficients ($D_{fluid\text{-}melt}$) for REE are higher for peraluminous melts compared to metaluminous and peralkaline melts and increase with peraluminosity (London et al., 1988; Borchert et al., 2010). They also increase with a pressure drop (Flynn and Burnham, 1978; Webster et al., 1989; Bai and Van Groos, 1999) and strongly increase with increasing Cl concentrations of the fluids (Webster et al., 1989; Reed et al., 2000; Borchert et al., 2010). Chlorine always partitions into the fluid over the melt, and the partition coefficient for Cl ($D^{Cl}_{fluid\text{-}melt}$) increases with increasing temperature and peraluminosity of the melt, while it decreases with increasing F concentration of the melt (Webster and Holloway, 1988). At 650 °C, REE partitioning into the fluid is about 50% stronger than at 775 °C in peraluminous melts (London et al., 1988). Phosphorous favours the melt over the fluid, but the partitioning of P to the fluid is one magnitude higher in peraluminous compared to metaluminous systems, and P usually has a higher or a similar partition coefficient as the REE (London et al., 1988; 1993). The most suitable conditions for partitioning of REE and P into the fluids should thus be in peraluminous systems exsolving high-salinity fluids, possibly at temperatures of about 650 °C. These conditions coincide well with that of the Olserum-Djupedal REE-mineralising system.

The detailed exposition about the P and REE concentrations of felsic melts and fluid-melt partitioning of REE and P serves to illustrate that a fractionating peraluminous granitic system has a great potential to exsolve fluids relatively enriched in REE and P. Fluid exsolution at an early stage for the Olserum-Djupedal REE mineralisation, as proposed in Paper II, is also advantageous because the ore-forming fluid will have more time to interact and scavenge REE and P from minerals (potentially early-crystallised monazite-(Ce) and xenotime-(Y)) and from the melt. In addition, if fluid saturation occurs early, the F concentration of the melt will be relatively low because of limited fractionation, and $D^{Cl}_{fluid\text{-}melt}$ remains high (Audétat et al., 2000). Thus, low REE and P_2O_5 concentrations of the granite do not imply low REE and P concentrations of the peraluminous melt at the time of primary REE mineralisation, but rather resulted from a combination of fluid exsolution, melt heterogeneities and late pegmatite extraction. In other silicate systems, low solubility of apatite will lead to early crystallisation of apatite during fractionation, removing most of the P in the system. Lower

REE and P fluid-melt partition coefficients in such systems also indicate a lower potential for the exsolution of REE-P-rich fluids.

In hydrothermal REE deposits not related to any known igneous activity such as xenotime-(Y)-rich unconformity-related REE deposits (Vallini et al., 2007; Rabiei et al., 2017; Nazari-Dehkordi et al., 2018; Richter et al., 2018), REE and P are probably transported in separate fluids. The source of P is likely from P-enriched sedimentary beds such as phosphorites, which also can contain high concentrations of REE (Emsbo et al., 2015), while REE originate from the alteration of basement rocks (Nazari-Dehkordi et al., 2018).

5.3 Hydrothermal transport of REE and P and precipitation of REE-phosphate minerals

Transport of REE in a fluid requires the formation of stable metal complexes with available ligands in the fluid at the specific conditions of the hydrothermal system to keep the REE in solution. Recent experimental studies on the stabilities of different REE complexes at elevated temperatures (up to 250 °C) and geochemical modelling show that significant REE transport primarily occurs by REE-Cl complexes ($REECl^{2+}$ and $REECl_2^{+}$) only at acidic conditions in Cl-F-bearing fluids (e.g., Migdisov et al., 2009, 2014, 2016). Addition of the SO_4^{2-} ligand expands the pH range in which the REE can be transported, especially at higher temperatures (300-400 °C) due to the formation of stable $REE(SO_4)^{2-}$ (Migdisov et al., 2016). In F-free fluids, the REE can be transported at neutral conditions to slightly alkaline conditions with the addition of SO_4^{2-} (Migdisov et al., 2016), or even at alkaline conditions by REE-OH complexes (Wood et al., 2002; Pourtier et al., 2010; Perry and Gysi, 2018). The reduced solubilities for the REE at higher pH in F-bearing fluids are thought to originate because of the increased dissociation of HF at increasing pH (Fig. 7), which results in more F ions being able to bind with the REE until the fluid reaches $REEF_3$(s) saturation (Williams-Jones et al., 2012; Migdisov et al., 2016). However, $REEF_3$ minerals are rare in nature, but the point is rather that insoluble REE-F-bearing minerals, for example, bastnäsite-(Ce), may govern the availability of REE in hydrothermal fluids at increasing pH. However, it is also possible that high stabilities of REE-OH-F complexes at high pH can inhibit saturation of $REEF_3$(s) or other REE-F-bearing minerals and retain the REE in solution (Vasyukova and Williams-Jones, 2018). To precipitate the REE as REE-bearing minerals, a process or processes are required to drive the system into conditions that promote REE mineral formation instead of favouring REE complexation. Based on geochemical modelling (Migdisov and Williams-Jones, 2014; Migdisov et al., 2016), possible mechanisms to induce REE precipitation are 1) pH-changes, 2) introduction of binding ligands, 3) destabilisation of REE-transporting complexes, or 4) cooling.

Phosphorous, as phosphate, is considered a strong binding ligand in REE-mineralising systems and probably contribute nothing to the transport of REE. This has been inferred based on the low and retrograde solubilities of monazite and xenotime at temperatures up to 300 °C in acidic solutions ($pH \leq 2$; cf., Poitrasson et al., 2004; Cetiner et al., 2005; Gysi et al., 2015; 2018; Migdisov et al., 2016). Modelling shows that when phosphate is introduced into the hydrothermal system, either by fluid-rock interaction with P-enriched rocks or by mixing with P-enriched fluids, the REE in the solution will immediately react with phosphate and precipitate monazite or xenotime. This is probably a very efficient precipitation mechanism when REE and P are not transported by the same fluid. Pourtier et al. (2010) suggested that monazite solubility

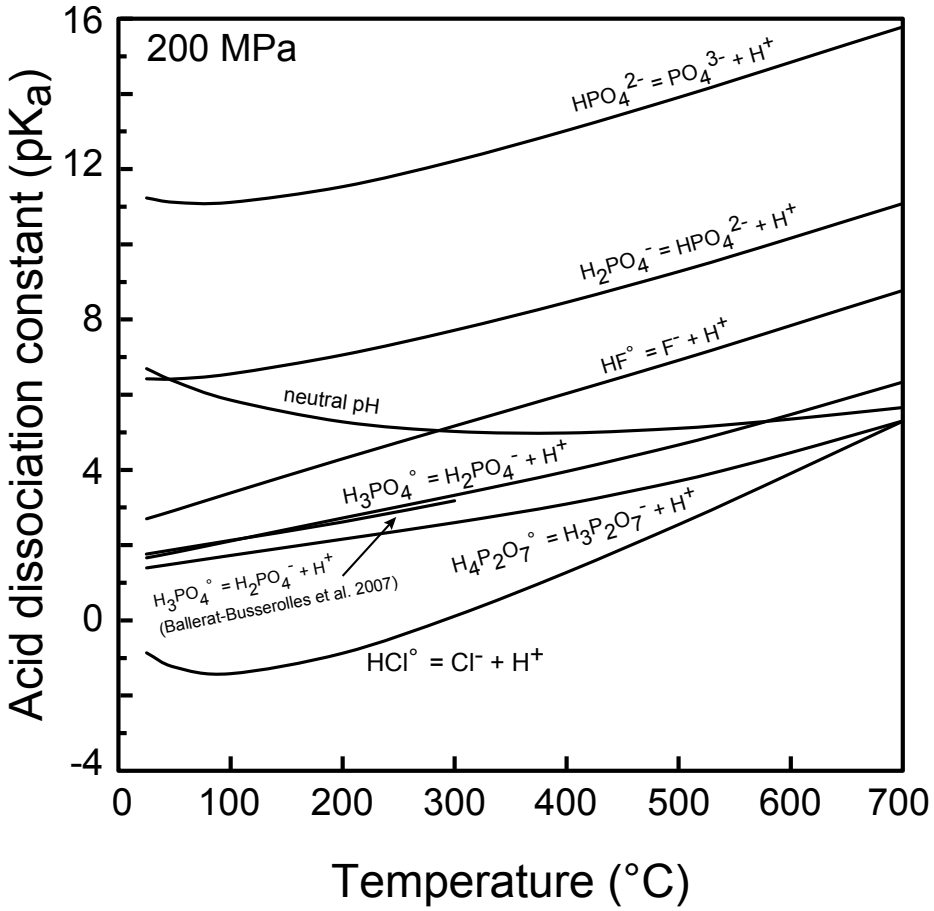

Fig. 7. A diagram showing the acid dissociation constant (pK_a) for the reactions involving the common phosphate species ($H_3PO_4^\circ$, $H_2PO_4^-$, and HPO_4^{2-}), HCl°, and HF° as an effect of temperature at 200 MPa. The blue line shows how the neutral pH changes with temperature. Calculated using data from the SUPCRT92 database (Johnson et al., 1992) and complementary data from Shock et al. (1997) and Tagirov et al. (1997). At pK_a, the activities of dissociated (e.g., $H_3PO_4^\circ$) and associated (e.g., $H_2PO_4^-$) species are equal. When pH > pK_a, the dissociated species predominate.

is prograde at least from 300 to 800 °C at more neutral pH, which indicates that REE may be complexed with phosphate at higher temperatures, or that phosphate is co-transported with REE in the fluid and the REE are complexed with other ligands (e.g., OH^-). This supports the study of Ague (2017), who demonstrated a strong correlation between REE and P mobility during regional metamorphism in crustal and subduction zone environments.

A recent attempt to model the mobility of REE (along with Fe and U) by F-bearing fluids in rock-buffered granitic-hydrothermal environments and at conditions approximating those of the Olserum-Djupedal REE-mineralising system (Xing et al., 2019) showed that:

1) The solubility of La was higher in F-bearing fluids compared to F-free fluids because of the stability of LaF^{2+}.

2) The pH of F-bearing fluids decreases with increased temperature and salinity. For a salinity exceeding 2 m (~10 wt% NaCl) and a temperature over 400 °C, the pH of the F-bearing fluids is lower than that of F-free fluids. This directly affects the solubilities of REE as the REE are more soluble at lower pH.

3) The soluble P concentration is in general higher for F-free fluids compared to F-bearing fluids. However, at temperatures above ~400 °C and salinities exceeding 10 wt% NaCl, the concentration of P is higher for F-bearing fluids than for F-free fluids. It also seems that the difference between the soluble P concentration in F-bearing fluids relative to F-free fluids increases with increasing temperature, even beyond the maximum temperature of 450 °C for the model.

These results suggest that co-transport of REE (as F- and Cl-complexes) and P can occur in acidic fluids with a salinity greater than 10 wt% NaCl at temperatures above 400 °C. These conditions also coincided with the highest solubility of Fe in F-bearing fluids. The rock-buffered concentration of La in the fluid is ~1 ppm. If compared to various magmatic-hydrothermal REE-bearing fluids (Table 2), this concentration is similar to some low to intermediate salinity fluids from the Strange Lake REE deposit and other magmatic-hydrothermal systems. However, it is one magnitude lower than compared with many brine inclusions, especially the extremely high-salinity "fluids" at Capitan Mountain and associated REE mineralisation (Table 2; Banks et al., 1994; Campbell et al., 1995; Audétat et al., 2008). Soluble P concentration in the model by Xing et al. (2019) is low, 10^{-3} to 10^{-4} ppm. However, in vapour/melt experiments for peraluminous granitic systems, concentrations of P and of individual REE in the co-existing vapour phase were ~400 ppm and ~0.2 ppm, respectively (London et al., 1988). This indicates that exsolved magmatic fluids from peraluminous granitic systems can contain elevated P concentrations.

In summary, high capability for co-transport of REE and P in F-bearing fluids seems most probable with increasing salinity of the fluids and at temperatures above 400 °C. Moreover, co-transport of REE and P primarily occurs at acidic conditions but depending on the stabilities of REE-OH-F complexes at these temperatures, co-transport of REE and P may be feasible even at neutral to alkaline conditions (cf., Vasyukova and Williams-Jones, 2018). The low solubilities of monazite and xenotime in acidic fluids at temperatures below 300 °C (Poitrasson et al., 2004; Cetiner et al., 2005; Gysi et al., 2015; 2018; Migdisov et al., 2016) likely preclude co-transport of REE and P at those conditions. In F-free fluids, co-transport of REE and P are also probable to more neutral or alkaline conditions, particularly with increasing temperatures up to 800 °C. An evaluation of different mechanisms that can precipitate REE-phosphates can thus be made:

1) pH change; changes in pH of the solution would be achieved by for instance fluid-rock interaction with a suitable rock or mixing with a fluid of different pH (Migdisov and Williams-Jones, 2014; Migdisov et al., 2016). At acidic pH, P mostly occurs as associated $H_3PO_4^\circ$ or possibly as $H_4P_2O_7^\circ$ at high P concentration (P ~ 0.1 molal or 0.3 wt% P; Pourtier et al., 2010). When pH increases, $H_3PO_4^\circ$ (and $H_4P_2O_7^\circ$) become increasingly dissociated and more $H_2PO_4^-$ ions (and $H_3P_2O_7^-$ ions) will dominate. For instance, at 500 °C and 200 MPa, pKa is 4.7 for $H_3PO_4^\circ$ (and 3.7 for $H_4P_2O_7^\circ$; neutral pH is at 5.1 at these conditions; Fig. 7). Thus, if the REE- and P-bearing fluids initially were rather acidic, the fluid will get increasingly richer in dissociated ions upon neutralisation until it eventually reaches saturation with respect to $REEPO_4$(s). When this occurs is strongly controlled by the solubility product of $REEPO_4$(s), which also will depend on the initial concentrations of REE^{3+} and P in the fluid. $REEPO_4$(s) saturation is also controlled by the stabilities of REE complexes at higher pH (e.g., REE-OH complexes), which may retain the REE in solution. Additional components in the fluid such as F (or CO_2) will determine if

Table 2. Compilation of REE concentrations of different magmatic-hydrothermal fluids.

Locality	Type	Salinity (wt% NaCl eq.)	Homogenisation temperature	Major elements	REE concentrations (ppm)	References
Bajo de la Alumbrera, Argentina	Porphyry Cu-Au deposit	37-70	300-750 °C	Na, Fe, K, Mn	La: 4-150 (430[1], brine) Ce: 1-30 (210[1], brine)	Ulrich et al. (2002)
Baveno, Italy	Peraluminous granites (A/CNK = 1.06-1.17), miarolitic cavities	5.9	380 °C	Na, K, Al, Fe	La: 1.7 (low-salinity) Ce: 9 (low-salinity)	Zajacz et al. (2008)
Canada Pinabete, Mexico	Metaluminous granite (A/CNK = 0.98-1.02), miarolitic cavities	4-5	410 °C	Na, K, (Fe, Al)	Ce: 2.4 (low-salinity), 100 (brine)	Audétat and Pettke (2003)
Capitan Mt., USA	(Alkali)-granite with Th-U-REE mineralisation	2.2, 62.7-80.4	590-650 °C	Na, K, Fe, Mn, Ca	La: 70-330 (brine) Ce: 13 (low-salinity), 80-580 (brine)	Banks et al. (1994); Campbell et al. (1995); Audétat et al. (2008)
Cave Peak, USA	Porphyry Mo-Nb-(Cu-W)	2.7-6.2, 38-2-49.7	450-600 °C	Na, K, Fe	Ce: <12 (low-salinity), 4-180 (brine)	Audétat et al. (2008)
Copper Flat, USA	Porphyry Cu-Mo deposit	16.7-21.9	189-390	Na, K, Fe	La: 2.8-71 (intermediate salinity) Ce: 2.8-89 (intermediate salinity)	Norman et al. (1989)
Cuasso al Monte, Italy	Peraluminous granites (A/CNK = 1.06-1.17), miarolitic cavities	53-69	450-570 °C	Na, K, Fe, Mn	La: 9.4 (brine) Ce: 21.4 (brine)	Zajacz et al. (2008)
Ehrenfriedersdorf, Germany	Strongly peraluminous, high F and P_2O_5, and Li-mica granites	7-8.5	> 400 °C	Na, K, Al, Fe, Cu	Ce: 2.1 (low-salinity)	Zajacz et al. (2008)
Mole, Australia	S-type granite with Sn-W-(Cu-Ag-Pb-Zn) and W-(Bi) mineralisations	3.1-6.3, 28.1-52	400-620 °C	Na, K, Fe, (Mn)	Ce: 0.1-48 (low-salinity), 1-17 (brine)	Audétat et al. (2008)
Mt. Malosa, Malawi	Alkali pegmatite, miarolitic cavities with REE and HFSE minerals	6.5-15, 31.5-35	350-550 °C	Na, K, Fe	La: 2.1-3.7 (low-salinity), 1.2-4.2 (brine) Ce: 3.2-11 (low-salinity), 1.3-5 (brine)	Zajacz et al. (2008)
Rito del Medio, Mexico	Metaluminous granite (A/CNK = 0.98-1.02), miarolitic cavities	3.7-7.5, 26-29.6	420-480 °C	Na, K, Fe, Mn	La: 1.3-2.9 (low-salinity) Ce: 1.1-5 (low-salinity; 1-5 (brine)	Audétat and Pettke (2003); Audétat et al. (2008); Zajacz et al. (2008)
Santa Rita, USA	Porphyry Cu-(Mo-Au)	10-21.7, 31.9-33.1	650-720 °C	Na, K, Fe, (Mn, Cu)	Ce: <24 (low-salinity), 6-16 (brine)	Audétat et al. (2008)
Strange Lake, Canada	Peralkaline granite associated with REE mineralisation	4-23	150-420 °C	Na, Ca, (K)	La: 1-7.4 (low- to intermediate salinity) Ce: 3.1-15 (low- to intermediate salinity)	Vasyukova and Williams-Jones (2018)
Stronghold, USA	Alkalic granite, Zn-Pb-Cu mineralisation	1-6.2, 26.3-31.6	400-510 °C	Na, K, Fe	Ce: 0.5-3 (low-salinity), <8 (brine)	Audétat et al. (2008)
Okorusu, Namibia	Carbonatite			Na, K, Ca, Fe, CO_2	La: 9200-13300 (normalised), 10.5[2] Ce: 11400-17200 (normalised), 13.5[2]	Bühn et al. (2002)
Kalkfeld, Namibia	Carbonatite			Na, K, Ca, Fe, CO_2	La: 3360-18900 (normalised), 25.3[2] Ce: 3800-12800 (normalised), 20.5[2]	Bühn and Rankin (1999)
Olserum-Djupedal, Sweden	Peraluminous granite (A/CNK = 1.05-1.11)	~45	~300 °C	Na, Fe, K, Ca	Ce: 0.85-1.25 (brines)	This study (Table A2)

[1] Represents one outier

[2] Aveage concentratioons of quartz and leachate

the fluid will become saturated with $REEF_3$(s) (or possible REE-fluorocarbonates) instead of $REEPO_4$(s) with increasing pH. As the solubility of $REEPO_4$(s) thus is dependent on temperature, pH, stabilities of REE complexes, and the concentrations of different elements in the fluid (e.g., Cl, F, P, and S), all these parameters need to be considered for a specific hydrothermal REE-mineralising system if precipitation by changes in the pH is a feasible precipitation mechanism or not.

2) The destabilisation of REE-transporting complexes; because $REECl^{2+}$ and $REECl_2^+$, and in some fluids, $REEF^{2+}$, or $REESO_4^+$ and $REE(SO_4)^{2-}$, or $REE(OH)_3^\circ$ and $REE(OH)_2^+$, are the chief REE transporting agents, destabilising these will decrease the solubility of REE and saturate the solution in $REEPO_4$(s). To destabilise REE-Cl complexes, mixing with fluids of lower salinity such as metamorphic or meteoric fluids will dilute the REE-transporting fluid and thus the ability to dissolve the REE (Migdisov et al., 2016). If the REE-transporting fluid contains high S concentration, transport of REE by REE-SO_4 complexes are very likely. The destabilisation of these complexes could be effectively achieved by precipitation of insoluble barite, or by the reduction of SO_4 to sulphide or other reduced species (Migdisov et al., 2016). A decrease of F in the fluid by precipitating minerals exhibiting a strong preference for F such as fluorapatite (Zhu and Sverjensky, 1991; Spear and Pyle, 2002; Harlov, 2015; Kusebauch et al., 2015a, 2015b) will effectively destabilise REE-F complexes and Th-F and (Nb,Ta)-F complexes. This could be responsible for the formation of REE-(Nb,Ta) oxides in the Olserum-Djupedal REE mineralisation. The destabilisation REE-OH complexes may be achieved by fluid mixing with a lower pH-fluid. However, if $REEPO_4$(s) saturation occurs will be highly dependent on the concentrations of other elements in the fluid, and the stabilities of their respective REE-complexes.

3) Cooling generally reduces the solubility of REE in fluids by the lowering the stabilities of transporting REE complexes (e.g., Migdisov et al., 2016). Cooling also decreases the solubility of monazite in neutral-pH fluids at temperatures between 300 and 800 °C (Pourtier et al., 2010). Cooling also increases the dissociation of $H_3PO_4^0$ at constant pH. Cooling, however, also increases the availability of the important REE complexing ligands Cl^- and F^- due to the increased dissociation of HCl° and HF° species. These competing factors thus dictate whether saturation of the fluid with $REEPO_4$(s) will occur during cooling.

4) Introduction of phosphate ligand; very efficient precipitation mechanism if REE and P are not co-transported or if a REE-bearing fluid interacts with P-enriched lithologies. Yet, even if REE and P are co-transported, with additional P added to the solution, it would probably reach saturation of $REEPO_4$(s) earlier. One potential limitation with this mechanism is identifying the rock type or fluid that are sufficiently enriched in P to facilitate this process. In carbonatite-silicate systems, such a rock could potentially be early apatite cumulates or apatite-rich carbonatites (Zaitsev et al., 2015; Chakhmouradian et al., 2017, and references therein). In such systems, fluid-interaction with early formed apatite is likely the most important precipitation mechanism. In other hydrothermal systems, however, it could be challenging to recognise pre-existing P-enriched rocks. A joint source of REE and P may thus be more common than not in many magmatic-hydrothermal systems. In low-temperature systems such as unconformity-related REE deposits, co-transport of REE and P is unlikely, and they are probably transported in separate fluids. Some specific basinal fluids can be P-enriched, and xenotime precipitates when the REE-bearing fluid mixes with the basinal P-enriched fluid (Nazari-Dehkordi et al., 2018).

5.4 Outlook and remaining research topics

Although the approach of this research project has shifted slightly from the original idea, the purpose has stayed the same; to contribute to the understanding of how hydrothermal REE deposits form. The main goal was to identify the main REE-transporting agents in hydrothermal REE systems by determining the compositions of REE-bearing fluids and to use geochemical modelling to identify key depositional mechanisms. While this goal has partially been reached, this study has primarily contributed to the understanding and recognition of a new and potentially regional-scale hydrothermal REE system, and the implications this have had on the general understanding of hydrothermal REE-mineralising systems.

Modelling of hydrothermal REE-mineralising systems has aptly been made in several studies in recent years (Migdisov and Williams-Jones, 2014; Migdisov et al., 2016; 2018; Perry and Gysi, 2018; Xing et al., 2019). These studies have laid the foundation for the understanding of REE transport and precipitation of REE-bearing minerals. However, the models have not considered co-transport of REE and P. This is mainly because of the general lower temperatures used for these models. This is, however, a direct consequence of the lack of experimental studies at the relevant conditions where co-transport of REE and P is likely to occur.

Additional experimental data are thus required before new geochemical modelling can be conducted. Such new models should also consider high-temperature conditions, which would be applicable to the Olserum-Djupedal REE-mineralising system. For instance, studies on the solubilities of monazite, xenotime and the apatite end-members as well as other REE-bearing minerals (e.g., bastnäsite) in addition to studies on the stabilities of different REE complexes (including PO_4-complexes) at magmatic-hydrothermal conditions would be extremely desirable. Constraints on the concentration of P in magmatic-hydrothermal fluids of different affinity would be vital in order to model the formation of hydrothermal REE-phosphate deposits. Likewise, reliable concentrations of individual REE in magmatic-hydrothermal fluids, and of other potential ore-forming fluids, would also be highly desirable. At that point would it be possible to make better predictions on how REE are transported in crustal fluids and how REE deposits form in various hydrothermal settings.

6 Conclusions

This study has foremost focused on understanding the origin and evolution of the Olserum-Djupedal REE mineralisation in SE Sweden. The mineralisation is unique in many aspects, like in the paragenesis and style, and hosts abundant monazite-(Ce), xenotime-(Y) and variably REE-bearing fluorapatite. The main findings and implications of the study can be summarised as follows:

I. Primary REE mineralisation in the Olserum-Djupedal district formed at magmatic-hydrothermal conditions (~600 °C) by magmatic NaCl-$FeCl_2$-KCl-$CaCl_2$-HF-H_2O fluids at c. 1.8 Ga. During subsequent cooling, the ore assemblages were variably altered by $CaCl_2$-NaCl to NaCl-$CaCl_2$ brines and partly by CO_2-bearing fluids down to temperatures of around 300 °C and to at least 1.75 Ga.

II. Co-crystallisation of fluorapatite, monazite-(Ce) and xenotime-(Y) in the Olserum-Djupedal REE mineralisation and lack of rocks pre-enriched in terms of P suggest a

joint source of REE and P. There is no need to invoke a scenario where REE and P are transported by separate fluids.

III. High capability for co-transport of REE and P is most probable at increasing salinity of the hydrothermal fluids and at increasing temperatures above 400 °C. Acidic conditions would make the co-transport of REE and P more effective. Yet, depending on the stabilities of REE-OH complexes at these temperatures, co-transport of REE and P may be feasible even at neutral to alkaline conditions. Additional constituents in the fluid such as F, S and, CO_2 will also influence the co-transporting ability of the fluid.

IV. While hydrothermal REE mineralisations are typically related to alkaline magmatism, particularly to alkaline silicate-carbonatitic systems, this study shows that high-grade hydrothermal REE-mineralising systems can also develop in association with subalkaline magmatism. Out of the subalkaline granitic systems, fractionating peraluminous granites show the greatest potential to exsolve fluids carrying REE and P, which can lead to the formation of hydrothermal REE deposits rich in REE-bearing phosphates.

V. REE-phosphate precipitation by the interaction of a REE-bearing fluid with a P-rich rock or fluid is a very efficient mechanism at conditions where co-transport of REE and P are improbable. In fluids co-transporting REE and P, cooling, pH changes or the destabilisation of the main REE transporting agents, or more viably, a combination of these are likely the most prominent mechanisms precipitating REE-phosphates.

References

Ague, J.J., 2017. Element mobility during regional metamorphism in crustal and subduction zone environments with a focus on the rare earth elements (REE). Am. Mineral. 102, 1796–1821.

Åhäll, K.I., Larson, S.Å., 2000. Growth-related 1.85-1.55 Ga magmatism in the Baltic Shield; a review addressing the tectonic characteristics of Svecofennian, TIB 1-related, and Gothian events. GFF 122, 193–206.

Andersen, T., 1986. Compositional variation of some rare earth minerals from the Fen complex (Telemark, SE Norway): implications for the mobility of rare earths in a carbonatite system. Mineral. Mag. 50, 503–9.

Andersen, T., Andersson, U.B., Graham, S., Aberg, G., Simonsen, S.L., 2009. Granitic magmatism by melting of juvenile continental crust: new constraints on the source of Palaeoproterozoic granitoids in Fennoscandia from Hf isotopes in zircon. J. Geol. Soc. London. 166, 233–247.

Andersson, U.B., Wikström, A., 2001. Growth-related 1.85-1.55 Ga magmatism in the Baltic shield; a review addressing the tectonic characteristics of Svecofennian, TIB 1-related, and Gothian events. GFF 123, 55–58.

Audétat, A., Pettke, T., 2003. The magmatic-hydrothermal evolution of two barren granites: a melt and fluid inclusion study of the Rito del Medio and Canada Pinabete plutons in northern New Mexico (USA). Geochim. Cosmochim. Acta 67, 97–121.

Audétat, A., Günther, D., Heinrich, C.A., 2000. Magmatic-hydrothermal evolution in a fractionating granite: a microchemical study of the Sn-W-F-mineralized mole granite (Australia). Geochim. Cosmochim. Acta 64, 3373–3393.

Audétat, A., Pettke, T., Heinrich, C.A., Bodnar, R.J., 2008. Special paper: The composition of magmatic-hydrothermal fluids in barren and mineralized intrusions. Econ. Geol. 103, 877–908.

Audi, G., Bersillon, O., Blachot, J., Wapstra, A.H., 2003. The NUBASE evaluation of nuclear and decay properties. Nucl. Phys. A 729, 3–128.

Bai, T.B., Koster Van Groos, A.F., 1999. The distribution of Na, K, Rb, Sr, Al, Ge, Cu, W, Mo, La, and Ce between granitic melts and coexisting aqueous fluids. Geochim. Cosmochim. Acta 63, 1117–1131.

Ballerat-Busserolles, K., Sedlbauer, J., Majer, V., 2007. Standard thermodynamic properties of H_3PO_4(aq) over a wide range of temperatures and pressures. J. Phys. Chem. B 111, 181–190.

Banks, D.A., Yardley, B.W.D., Campbell, A.R., Jarvis, K.E., 1994. REE composition of an aqueous magmatic fluid: a fluid inclusion study from the Capitan Pluton, New Mexico, U.S.A. Chem. Geol. 113, 259–272.

Banks, D.A., Gleeson, S.A., Green, R., 2000a. Determination of the origin of salinity in granite-related fluids: evidence from chlorine isotopes in fluid inclusions. J. Geochem. Explor. 69-70, 309–312

Banks, D.A., Green, R., Cliff, R.A., Yardley, B.W.D., 2000b. Chlorine isotopes in fluid inclusions: determination of the origins of salinity in magmatic fluids. Geochim. Cosmochim. Acta 64, 1785–1789.

Bea, F., Fershtater, G., Corretgé, L.G., 1992. The geochemistry of phosphorus in granite rocks and the effect of aluminium. Lithos 29, 43–56.

Bea, F., Pereira, M.D., Corretgé, L.G., Fershtater, G.B., 1994. Differentiation of strongly peraluminous, perphosphorus granites: the Pedrobernardo pluton, central Spain. Geochim. Cosmochim. Acta 58, 2609–2627.

Bergström, U., Juhojuntti, N., Kero, L., Lundqvist, L., Stephens, M.B., Sukotjo, S., Wik, N.G., Wikman, H., 2002. Projekt Småland, regionalt berg. In: Delin, H. (Ed.), Regional berggrundsgeologisk undersökning. Sammanfattning av pågående undersökningar 2001. Sveriges Geologiska Undersökning Rapporter och Meddelanden 110, pp. 65–83.

Beunk, F.F., Page, L.M., 2001. Structural evolution of the accretional continental margin of the Paleoproterozoic Svecofennian orogen in Southern Sweden. Tectonophysics 339, 67–92.

Billström, K., Broman, C., Söderhielm, J., 2004. The Solstad Cu ore - an Fe oxide-Cu-Au type deposit in SE Sweden. GFF 126, 147–148.

Bodeving, S., Williams-jones, A.E., Swinden, S., 2017. Carbonate–silicate melt immiscibility, REE mineralising fluids, and the evolution of the Lofdal Intrusive Suite, Namibia. Lithos 268–271, 383–398.

Bodnar, R.J., 1993. Revised equation and table for determining the freezing point depression of H_2O-NaCl solutions. Geochim. Cosmochim. Acta 57, 683–684.

Böhlke, J.K., Irwin, J.J., 1992. Laser microprobe analyses of Cl, Br, I, and K in fluid inclusions: implications for sources of salinity in some ancient hydrothermal fluids. Geochim. Cosmochim. Acta 56, 203–225.

Boily, M., Williams-Jones, E., 1994. The role of magmatic and hydrothermal processes in the chemical evolution of the Strange Lake plutonic complex, Québec-Labrador. Contrib. to Mineral. Petrol. 118, 33–47.

Boness, M., Heumann, K.G., Haack, U., 1991. Cl, Br and I analyses of metamorphic and sedimentary rocks by isotope dilution mass spectrometry. Contrib. Miner. Pet. 107, 94–99.

Borchert, M., Wilke, M., Schmidt, C., Cauzid, J., Tucoulou, R., 2010. Partitioning of Ba, La, Yb and Y between haplogranitic melts and aqueous solutions: an experimental study. Chem. Geol. 276, 225–240.

Bühn, B., Rankin, A.H., 1999. Composition of natural, volatile-rich Na–Ca–REE−Sr carbonatitic fluids trapped in fluid inclusions. Geochim. Cosmochim. Acta 63, 3781–3797.

Bühn, B., Rankin, A.H., Schneider, J., Dulski, P., 2002. The nature of orthomagmatic, carbonatitic fluids precipitating REE,Sr-rich fluorite: fluid-inclusion evidence from the Okorusu fluorite deposit, Namibia. Chem. Geol. 186, 75–98.

Campbell, A.R., Banks, D.A., Phillips, R.S., Yardley, B.W.D., 1995. Geochemistry of Th-U-REE mineralizing magmatic fluids, Capitan Mountains, New Mexico. Econ. Geol. 90, 1271–1287.

Castor, S.B., Hendrick, J.B., 2006. Rare Earth Elements. Ind. Miner. Rocks Commod. Mark. Uses, 769–792.

Cetiner, Z.S., Wood, S.A., Gammons, C.H., 2005. The aqueous geochemistry of the rare earth elements. Part XIV. The solubility of rare earth element phosphates from 23 to 150C. Chem. Geol. 217, 147–169.

Chakhmouradian, A.R., Zaitsev, A.N., 2012. Rare earth mineralization in igneous rocks: sources and processes. Elements 8, 347–353.

Chakhmouradian, A.R., Reguir, E.P., Zaitsev, A.N., Couëslan, C., Xu, C., Kynický, J., Mumin, A.H., Yang, P., 2017. Apatite in carbonatitic rocks: compositional variation, zoning, element partitioning and petrogenetic significance. Lithos 274–275, 188–213.

Chen, W.T., Zhou, M.F., 2015. Mineralogical and geochemical constraints on mobilization and mineralization of rare earth elements in the Lala Fe-Cu-(Mo, REE) deposit, SW China. Am. J. Sci. 315, 671–711.

Collins, W.J., Beams, S.D., White, A.J.., Chappell, B.W., 1982. Nature and origin of A-Type granites with particular reference to southeastern Australia. Contrib. to Mineral. Petrol. 80, 189–200.

Delin, H., and Bastini, M., 2009, Bedrock map 111 Uppsala NO, scale 1:50 000. Sveriges geologiska undersökning K 145.

Djenchuraeva, R.D., Borisov, F.I., Pak, N.T., Malyukova, N.N., 2008. Metallogeny and geodynamics of the Aktiuz-Boordu Mining District, Northern Tien Shan, Kyrgyzstan. J. Asian Earth Sci. 32, 280–299.

Dostal, J., Kontak, D.J., Karl, S.M., 2014. The Early Jurassic Bokan Mountain peralkaline granitic complex (southeastern Alaska): geochemistry, petrogenesis and rare-metal mineralization. Lithos 202–203, 395–412.

Elbers, F.J., 1971. Evolution of the Svecofennian orogeny in the northeastern part of the Västervik area, southeastern Sweden, with special reference to deformation, metamorphism and magmatism. PhD thesis. Vrije University, Amsterdam.

Emsbo, P., McLaughlin, P.I., Breit, G.N., du Bray, E.A., Koenig, A.E., 2015. Rare earth elements in

sedimentary phosphate deposits: solution to the global REE crisis? Gondwana Res. 27, 776–785.

Flynn, R.T., Burnham, C.W., 1978. An experimental determination of rare earth partition coefficients between a chloride containing vapor phase and silicate melts. Geochim. Cosmochim. Acta 42, 685–701.

Fusswinkel, T., Wagner, T., Sakellaris, G., 2017. Fluid evolution of the Neoarchean Pampalo orogenic gold deposit (E Finland): constraints from LA-ICPMS fluid inclusion microanalysis. Chem. Geol. 450, 96–121.

Fusswinkel, T., Giehl, C., Beermann, O., Fredriksson, J.R., Garbe-Schönberg, D., Scholten, L., Wagner, T., 2018. Combined LA-ICP-MS microanalysis of iodine, bromine and chlorine in fluid inclusions. J. Anal. At. Spectrom. 33, 768–783.

Gaál, G., Gorbatschev, R., 1987. An outline of the Precambrian evolution of the Baltic shield. Precambrian Res. 35, 15–52.

Gavelin, S., 1984. The Västervik area in south-eastern Sweden. Studies in Proterozoic sedimentation, high-grade metamorphism and granitization. Sveriges Geologiska Undersökning Ba 32, 172 pp.

Goodenough, K.M., Schilling, J., Jonsson, E., Kalvig, P., Charles, N., Tuduri, J., Deady, E.A., Sadeghi, M., Schiellerup, H., Müller, A., Bertrand, G., Arvanitidis, N., Eliopolous, D.G., Shaw, R.A., Thrane, K., Keulen, N., 2016. Europe's rare earth element resource potential: an overview of metallogenetic provinces and their geodynamic setting. Ore Geol. Rev. 72, 838–856.

Gorbatschev, R., 2004. The Transscandinavian Igneous Belt – introduction and background. Geol. S. Finl. 37, 9–15.

Guillong, M., Meier, D.L., Allan, M.M., Heinrich, C.A., Yardley, B.W.D., 2008. SILLS: a MATLAB-based program for the reduction of laser ablation ICP-MS data of homogeneous materials and inclusions. Mineralogical Association of Canada Short Course Volumes 40, 328–333.

Gupta, C.K., Krishnamurthy, N., 2005. Extractive metallurgy of rare earths. CRC Press, Boca Raton, USA.

Gysi, A.P., Williams-Jones, A.E., 2013. Hydrothermal mobilization of pegmatite-hosted REE and Zr at Strange Lake, Canada: a reaction path model. Geochim. Cosmochim. Acta 122, 324–352.

Gysi, A.P., Williams-Jones, A.E., Harlov, D., 2015. The solubility of xenotime-(Y) and other HREE phosphates ($DyPO_4$, $ErPO_4$ and $YbPO_4$) in aqueous solutions from 100 to 250 °C and psat. Chem. Geol. 401, 83–95.

Gysi, A.P., Harlov, D., Miron, G.D., 2018. The solubility of monazite (CePO4), $SmPO_4$, and $GdPO_4$ in aqueous solutions from 100 to 250 °C. Geochim. Cosmochim. Acta 242, 143–164.

Haas, J.R., Shock, E.L., Sassani, D.C., 1995. Rare earth elements in hydrothermal systems: estimates of standard partial molal thermodynamic properties of aqueous complexes of the rare earth elements at high pressures and temperatures. Geochim. Cosmochim. Acta 59, 4329–4350.

Hammouda, T., Chantel, J., Devidal, J.L., 2010. Apatite solubility in carbonatitic liquids and trace element partitioning between apatite and carbonatite at high pressure. Geochim. Cosmochim. Acta 74, 7220–7235.

Harlov, D.E., 2015. Apatite: a fingerprint for metasomatic processes. Elements 11, 171–176.

Harrison, T.M., Watson, E.B., 1984. The behavior of apatite during crustal anatexis: equilibrium and kinetic considerations. Geochim. Cosmochim. Acta 48, 1467–1477.

Hatch, G.P., 2012. Dynamics in the global market for rare earths. Elements, 8, 341–346.

Haxel, G.B., Hedrick, J.B., Orris, G.J., 2002. Rare earth elements – critical resources for high technology. U.S. Geological Survey Fact Sheet, 087–02.

Hoeve, J., 1974. Soda metasomatism and radio-active mineralisation in the Västervik area, southeastern Sweden. PhD thesis, Vrije University, Amsterdam.

Hoeve, J., 1978. Composition and volume changes accompanying soda metasomatic alterations, Västervik area, SE Sweden. Geol. Rundsch. 67, 920–942.

Holser, W.T., 1979. Trace elements and isotopes in evaporites. Rev. Mineral. 6, 295–346.

Irwin, J.J., Roedder, E., 1995. Diverse origins of fluid in magmatic inclusions at Bingham (Utah, USA), Butte (Montana, USA), St. Austell (Cornwall, UK), and Ascension Island (mid-Atlantic, UK), indicated by laser microprobe analysis of Cl, K, Br, I, Ba + Te, U, Ar, Kr, and Xe. Geochim. Cosmochim. Acta 59, 295–312.

Jiang, S.Y., Wang, R.C., Xu, X.S., Zhao, K.D., 2005. Mobility of high field strength elements (HFSE) in magmatic-, metamorphic-, and submarine-hydrothermal systems. Phys. Chem. Earth. 30, 1020-1029.

Johnson, J.W., Oelkers, E.H., Helgeson, H.C., 1992. SUPCRT92: A software package for calculating the standard molal thermodynamic properties of minerals, gases, aqueous species, and reactions from 1 to 5000 bar and 0 to 1000 °C. Comp. Geosci. 18, 899-947.

Kaufmann, R., Long, A., Bentley, H., Davis, S., 1984. Natural chlorine isotope variations. Nature 309, 338–340.

Kendrick, M.A., Burgess, R., Pattrick, R.A.D., Turner, G., 2001. Fluid inclusion noble gas and halogen evidence on the origin of Cu-Porphyry mineralising fluids. Geochim. Cosmochim. Acta 65, 2651–2663.

Kendrick, M. A., Arculus, R., Burnard, P., Honda, M., 2013. Quantifying brine assimilation by submarine magmas: examples from the Galápagos

spreading centre and Lau Basin. Geochim. Cosmochim. Acta 123, 150–165.

Kendrick, M. A., Hémond, C., Kamanetsky, V. S., Danyushevsky, L., Devey, C. W., Rodemann, T., Jackson, M. G., Perfit, M. R., 2017. Seawater cycled throughout Earth's mantle in partially serpentinized lithosphere. Nat. Geosci. 10, 222–228.

Keppler, H., Wyllie, P.J., 1990. Role of fluids in transport and fractionation of uranium and thorium in magmatic processes. Nature 348, 531–533.

Keppler, H., Wyllie, P.J., 1991. Partitioning of Cu, Sn, Mo, W, U, and Th between melt and aqueous fluid in the systems haplogranite-H_2O-HCl and haplogranite-H_2O-HF. Contrib Miner. Pet. 109, 139–150.

Kleinhanns, I.C., Whitehouse, M.J., Nolte, N., Baero, W., Wilsky, F., Hansen, B.T., Schoenberg, R., 2015. Mode and timing of granitoid magmatism in the Västervik area (SE Sweden, Baltic Shield): Sr-Nd isotope and SIMS U-Pb age constraints. Lithos 212–215, 321–337.

Kovalenko, V.I., Tsaryeva, M., Goreglyad, A. V, Yarmolyuk, V. V, Troitsky, V.A., Hervig, R.L., Farmer, G.L., 1995. The peralkaline granite-related Khaldzan-Buregtey rare metal (Zr, Nb, REE) deposits, western Mongolia. Econ. Geol. 90, 530–547.

Kresten, P., 1986. The granites of the Västervik area, south-eastern Sweden. Sveriges Geologiska Undersökning C 814, 35 pp.

Kusebauch, C., John, T., Whitehouse, M.J., Engvik, A.K., 2015a. Apatite as probe for the halogen composition of metamorphic fluids (Bamble Sector, SE Norway). Contrib. Mineral. Petrol. 170, 34.

Kusebauch, C., John, T., Whitehouse, M.J., Klemme, S., Putnis, A., 2015b. Distribution of halogens between fluid and apatite during fluid-mediated replacement processes. Geochim. Cosmochim. Acta 170, 225–246.

Kynicky, J., Chakhmouradian, A., Xu, C., Krmicek, L., Galiova, M., 2011. Distribution and evolution of zirconium mineralization in peralkaline granites and associated pegmatites of the Khan Bogd complex, southern Mongolia. Can. Mineral. 49, 947–965.

Lecumberri-Sanchez, P., Bouabdellah, M., Zemri, O., 2018. Transport of rare earth elements by hydrocarbon-bearing brines: implications for ore deposition and the use of REEs as fluid source tracers. Chem. Geol. 479, 204–215.

Loges, A., Migdisov, A.A., Wagner, T., Williams-Jones, A.E., Markl, G., 2013. An experimental study of the aqueous solubility and speciation of Y(III) fluoride at temperatures up to 250 °C. Geochim. Cosmochim. Acta 123, 403–415.

London, D., 1992. Phosphorus in S-type magmas: the P_2O_5 content of feldspars from peraluminous granites, pegmatites, and rhyolites. Am. Mineral. 77, 126–145.

London, D., Hervig, R., Morgan, G., 1988. Melt-vapor solubilities and elemental partitioning in peraluminous granite-pegmatite systems: experimental results and Macusani glass at 200 MPa. Contrib. to Mineral. Petrol. 99, 360–373.

London, D., Morgan VI, G.B., Babb, H.A., Loomis, J.L., 1993. Behavior and effects of phosphorus in the system Na_2O-K_2O-Al_2O_3-SiO_2-P_2O_5-H_2O at 200 MPa(H_2O). Contrib. to Mineral. Petrol. 113, 450–465.

London, D., Wolf, M.B., Morgan VI, G.B., Garrido, M.G., 1999. Experimental silicate-phosphate equilibria in peraluminous granitic magmas, with a case study of the Alburquerque batholith at Tres Arroyos, Badajoz, Spain. J. Petrol. 40, 215–240.

Long, K.R., Van Gosen, B.S., Foley, N.K., Cordier, D., 2010. The principal rare earth elements deposits of the United States—a summary of domestic deposits and a global perspective. U.S. Geological Survey Scientific Investigations, Report 2010-5220, 96 pp.

Lottermoser, B.G., 1990. Rare-earth element mineralisation within the Mt. Weld carbonatite laterite, Western Australia. Lithos 24, 151–167.

Mansfeld, J., Beunk, F.F., Barling, J., 2005. 1.83-1.82 Ga formation of a juvenile volcanic arc–implications from U-Pb and Sm-Nd analyses of the Oskarshamn-Jönköping Belt, southeastern Sweden. GFF 127, 149-157.

Marien, C., Dijkstra, A.H., Wilkins, C., 2018. The hydrothermal alteration of carbonatite in the Fen Complex, Norway: mineralogy, geochemistry, and implications for rare earth element resource formation. Mineral. Mag. 82, 115–131.

Martin, L.H.J., Schmidt, M.W., Mattsson, H.B., Guenther, D., 2013. Element partitioning between immiscible carbonatite and silicate melts for dry and H_2O-bearing systems at 1-3 GPa. J. Petrol. 54, 2301–2338.

Massari, S., Ruberti, M., 2013, Rare earth elements as critical raw materials: focus on international markets and future strategies. Resour. Policy 38, 36–43.

McDonough, W.F., Sun, S.S., 1995. The composition of the Earth, Chem. Geol. 120, 223-253.

Migdisov, A.A., Williams-Jones, A.E., 2008. A spectrophotometric study of Nd(III), Sm(III) and Er(III) complexation in sulfate-bearing solutions at elevated temperatures. Geochim. Cosmochim. Acta 72, 5291–5303.

Migdisov, A.A., Williams-Jones, A.E., 2014. Hydrothermal transport and deposition of the rare earth elements by fluorine-bearing aqueous liquids. Miner. Depos 49, 987–997

Migdisov, A.A., Williams-Jones, A.E., Wagner, T., 2009. An experimental study of the solubility and speciation of the Rare Earth Elements (III) in fluoride- and chloride-bearing aqueous solutions at temperatures up to 300 °C. Geochim. Cosmochim. Acta 73, 7087–7109.

Migdisov, A., Williams-Jones, A.E., Brugger, J., and Caporuscio, F.A., 2016. Hydrothermal transport, deposition, and fractionation of the REE: experimental data and thermodynamic calculations. Chem. Geol. 439, 13–42.

Migdisov, A., Guo, X., Nisbet, H., Xu, H., Williams-Jones, A.E., 2018. Fractionation of REE, U, and Th in natural ore-forming hydrothermal systems: thermodynamic modeling. J. Chem. Thermodyn. 128, 305–319.

Mitchell, R.H., 2005. Carbonatites and carbonatites and carbonatites. Can. Mineral. 43, 2049–2068.

Mitchell, R.H., Smith, D.L., 2017. Geology and mineralogy of the Ashram Zone carbonatite, Eldor Complex, Québec. Ore Geol. Rev. 86, 784–806.

Möller, V., Williams-Jones, A.E., 2016. Petrogenesis of the Nechalacho layered suite, Canada: magmatic evolution of a REE-Nb-rich nepheline syenite intrusion. J. Petrol. 2, 229–276.

Möller, V., Williams-Jones, A.E., 2017. Magmatic and hydrothermal controls on the mineralogy of the basal zone, Nechalacho REE-Nb-Zr deposit, Canada. Econ. Geol. 112, 1823–1856.

Montel, J.-M., 1986. Experimental determination of the solubility of Ce-monazite in SiO_2-Al_2O_3-K_2O-Na_2O melts at 800 °C, 2 kbar, under H_2O-saturated conditions. Geology 14, 659–662.

Montel, J.-M., 1993. A model for monazite/melt equilibrium and application to the generation of granitic magmas. Chem. Geol. 110, 127–146.

Moore, M., Chakhmouradian, A.R., Mariano, A.N., Sidhu, R., 2015. Evolution of rare-earth mineralization in the Bear Lodge carbonatite, Wyoming: mineralogical and isotopic evidence. Ore Geol. Rev. 64, 499–521.

Navarro, J., Zhao, F., 2014. Life-Cycle Assessment of the production of rare-earth elements for energy applications: a review. Front. Energy Res. 2, 1–17.

Nazari-Dehkordi, T., Spandler, C., Oliver, N.H.S., Wilson, R., 2018. Unconformity-related rare earth element deposits: a regional-scale hydrothermal mineralization type of northern Australia. Econ. Geol. 113, 1297–1305.

Nolte, N., Kleinhanns, I.C., Baero, W., Hansen, B.T., 2011. Petrography and whole-rock geochemical characteristics of Västervik granitoids to syenitoids, southeast Sweden: constraints on petrogenesis and tectonic setting at the southern margin of the Svecofennian domain. GFF 133, 173–194.

Norman, D.I., Kyle, P.R., Baron, C., 1989. Analysis of trace elements including rare earth elements in fluid inclusions liquids. Econ. Geol. 84, 162–166.

North, J., 2008. Cosmos: an illustrated history of astronomy and cosmology. University of Chicago Press, Chicago, USA.

Paulick, H., Machacek, E., 2017. The global rare earth element exploration boom: an analysis of resources outside of China and discussion of development perspectives. Resour. Policy 52, 134–153.

Perry, E.P., Gysi, A.P., 2018. Rare earth elements in mineral deposits: speciation in hydrothermal fluids and partitioning in calcite. Geofluids 2018, 1–19.

Piccoli, P.M., Candela, P.A., 2002. Apatite in igneous systems. Rev. Mineral. Geochemistry 48, 255–292.

Pichavant, M., Montel, J.M., Richard, L.R., 1992. Apatite solubility in peraluminous liquids: experimental data and an extension of the Harrison-Watson model. Geochim. Cosmochim. Acta 56, 3855–3861.

Poitrasson, F., Oelkers, E., Schott, J., Montel, J.M., 2004. Experimental determination of synthetic $NdPO_4$ monazite end-member solubility in water from 21 °C to 300 °C: implications for rare earth element mobility in crustal fluids. Geochim. Cosmochim. Acta 68, 2207–2221.

Pourtier, E., Devidal, J.L., Gibert, F., 2010. Solubility measurements of synthetic neodymium monazite as a function of temperature at 2 kbars, and aqueous neodymium speciation in equilibrium with monazite. Geochim. Cosmochim. Acta 74, 1872–1891.

Pyle, J.M., Spear, F.S., Wark, D.A., 2002. Electron microprobe analysis of REE in apatite, monazite and xenotime: protocols and pitfalls. Rev. Mineral. Geochemistry 48, 337–362.

Rabiei, M., Chi, G., Normand, C., Davis, W.J., Fayek, M., Blamey, N.J.F., 2017. Hydrothermal rare earth element (xenotime) mineralization at Maw Zone, Athabasca Basin, Canada, and its relationship to unconformity-related uranium deposits. Econ. Geol. 112, 1483–1507.

Rapp, R.P., Ryerson, F.J., Miller, C.F., 1987. Experimental evidence bearing on the stability of monazite during crustal anatexis. Geophys. Res. Lett. 14, 307–310.

Reed, M.J., Candela, P.A., Piccoli, P.M., 2000. The distribution of rare earth elements between monzogranitic melt and the aqueous volatile phase in experimental investigations at 800 °C and 200 MPa. Contrib. to Mineral. Petrol. 140, 251–262.

Richter, L., Diamond, L.W., Atanasova, P., Banks, D.A., Gutzmer, J., 2018. Hydrothermal formation of heavy rare earth element (HREE)-xenotime deposits at 100 °C in a sedimentary basin. Geology 46, 263–266.

Rudnick, R.L., Gao, S., 2003. Composition of the continental crust. Treatise Geochemistry 3, 1–64.

Rukhlov, A.S., Bell, K., 2010. Geochronology of carbonatites from the Canadian and Baltic Shields, and the Canadian Cordillera: clues to mantle evolution. Mineral. Petrol. 98, 11–54.

Rutanen, H., Andersson, U.B., Väisänen, M., Johansson, Å., Fröjdö, S., Lahaye, Y., Eklund, O., 2011. 1.8 Ga magmatism in southern Finland: strongly enriched mantle and juvenile crustal sources in a post-collisional setting. Int. Geol. Rev. 53,

1622–1683.
Sarapää, O., Al Ani, T., Lahti, S.I., Lauri, L.S., Sarala, P., Torppa, A., Kontinen, A., 2013. Rare earth exploration potential in Finland. J. Geochemical Explor. 133, 25–41.
Schmandt, D., Cook, N., Ciobanu, C., Ehrig, K., Wade, B., Gilbert, S., Kamenetsky, V., 2017. Rare earth element fluorocarbonate minerals from the Olympic Dam Cu-U-Au-Ag deposit, South Australia. Minerals 7, 202.
Seo, J.H., Guillong, M., Aerts, M., Zajacz, Z., Heinrich, C.A., 2011. Microanalysis of S, Cl, and Br in fluid inclusions by LA-ICP-MS. Chem. Geol. 284, 35–44.
Shannon, R.D., 1976. Revised effective ionic radii and systematic studies of interatomic distances in halides and chalcogenides. Acta Crystallogr. A, 32, 751–767.
Shock, E.L., Sassani, D.C., Willis, M. Sverjensky, D.A., 1997. Inorganic species in geological fluids: correlations among standard molal thermodynamic properties of aqueous ions and hydroxide complexes. Geochim. Cosmochim. Acta 61, 907-950.
Sjöqvist, A.S.L., Cornell, D.H., Andersen, T., Erambert, M., Ek, M., Leijd, M., 2013. Three compositional varieties of rare-earth element ore: eudialyte-group minerals from the Norra Kärr Alkaline Complex, Southern Sweden. Minerals 3, 94–120.
Sjöqvist, A.S.L., Cornell, D.H., Andersen, T., Christensson, U.I., Berg, J.T., 2017. Magmatic age of rare-earth element and zirconium mineralisation at the Norra Kärr alkaline complex, southern Sweden, determined by U–Pb and Lu–Hf isotope analyses of metasomatic zircon and eudialyte. Lithos 294–295, 73–86.
Sørensen, H., Bohse, H., Bailey, J.C., 2006. The origin and mode of emplacement of lujavrites in the Ilímaussaq alkaline complex, South Greenland. Lithos 91, 286–300.
Spandler, C., Pettke, T., Rubatto, D., 2011. Internal and external fluid sources for eclogite facies veins in the Monviso meta-ophiolite, Western Alps: implications for fluid flow in subduction zones. J. Petrol. 52, 1207–1236.
Spear, F.S., Pyle, J.M., 2002. Apatite, monazite, and xenotime in Metamorphic Rocks. Rev. Mineral. Geochemistry 48, 293–335.
Steele-MacInnis, M., Bodnar, R.J., Naden, J., 2011. Numerical model to determine the composition of H_2O-NaCl-$CaCl_2$ fluid inclusions based on microthermometric and microanalytical data. Geochim. Cosmochim. Acta 75, 21–40.
Stock, M.J., Humphreys, M.C.S., Smith, V.C., Johnson, R.D., Pyle, D.M., 2015. New constraints on electron-beam induced halogen migration in apatite. Am. Mineral. 100, 281–293.
Stormer, J.C., Pierson, M.L., Tacker, R.C., 1993. Variation of F and Cl X-ray intensity due to anisotropic diffusion in apatite during electron microprobe analysis. Am. Mineral. 78, 641–648.
Sultan, L., Claesson, S., Plink-Björklund, P., 2005. Proterozoic and Archaean ages of detrital zircon from the Palaeoproterozoic Västervik Basin, SE Sweden: implications for provenance and timing of deposition. GFF 127, 17–24.
Sundblad, K., 2003. Metallogeny of gold in the Precambrian of Northern Europe. Econ. Geol. 98, 1271–1290.
Tagirov, B.R., Zotov, A. V., Akinfiev, N.N., 1997. Experimental study of dissociation of HCl from 350 to 500 °C and from 500 to 2500 bars: thermodynamic properties of HCl° (aq). Geochim. Cosmochim. Acta 61, 4267–4280.
Tegengren, F.R., 1924. Sveriges ädlare malmer och bergverk. Sveriges Geologiska Undersökning Ca 17, 406 pp.
Timofeev, A., Migdisov, A.A., Williams-Jones, A.E., 2015. An experimental study of the solubility and speciation of niobium in fluoride-bearing aqueous solutions at elevated temperature. Geochim. Cosmochim. Acta 158, 103–111.
Timofeev, A., Migdisov, A.A., Williams-Jones, A.E., 2017. An experimental study of the solubility and speciation of tantalum in fluoride-bearing aqueous solutions at elevated temperature. Geochim. Cosmochim. Acta 197, 294–304.
Trofanenko, J., Williams-Jones, A.E., Simandl, G.J., Migdisov, A.A., 2016. The nature and origin of the REE mineralization in the Wicheeda Carbonatite, British Columbia, Canada. Econ. Geol. 111, 199–223.
Ulrich, T., Gunther, D., Heinrich, C.A., 2002. The evolution of a Porphyry Cu-Au deposit, based on LA-ICP-MS analysis of fluid inclusions: Bajo de la Alumbrera, Argentina. Econ. Geol. 96, 1743–1774.
Uytenbogaardt, W., 1960. Uranium mineralization in the Västervik area. International Geological Congress 15, 114-122.
Vallini, D.A., Groves, D.I., McNaughton, N.J., Fletcher, I.R., 2007. Uraniferous diagenetic xenotime in northern Australia and its relationship to unconformity-associated uranium mineralisation. Miner. Depos. 42, 51–64.
Vanko, D.A., Bodnar, R.J., Sterner, S.M., 1988. Synthetic fluid inclusions: VIII. Vapor-saturated halite solubility in part of the system NaCl-$CaCl_2$-H_2O, with application to fluid inclusions from oceanic hydrothermal systems. Geochim. Cosmochim. Acta 52, 2451–2456.
Vasyukova, O.V., Williams-Jones, A.E., 2018. Direct measurement of metal concentrations in fluid inclusions, a tale of hydrothermal alteration and REE ore formation from Strange Lake, Canada. Chem. Geol. 483, 385–396.
Vasyukova, O.V., Williams-Jones, A.E., Blamey, N.J.F., 2016. Fluid evolution in the Strange Lake granitic pluton, Canada: implications for HFSE

mobilisation. Chem. Geol. 444, 83–100.
Wall, F. (2014) Rare earth elements. In Critical Metals Handbook, 312–339.
Wall, F., Niku-Paavola, V.N., Storey, C., Müller, A., Jeffries, T., 2008. Xenotime-(Y) from carbonatite dykes at Lofdal, Namibia: unusually low LREE:HREE ratio in carbonatite, and the first dating of xenotime overgrowths on zircon. Can. Mineral. 46, 861–877.
Watson, E.B., 1979. Apatite saturation in basic to intermediate magmas. Geophys. Res. Lett. 6. 937–940.
Watson, E.B., 1980. Apatite and phosphorus in mantle source regions: an experimental study of apatite/melt equilibria at pressures to 25 kbar. Earth Planet. Sci. Lett. 51, 322–335.
Watson, E.B., Capiobianco, C.J., 1981. Phosphorus and the rare earth element and assessment of the role of apatite. Geochimica Cosmochim. Acta 45, 2349–2358.
Webster, J.D., Holloway, J.R., 1988. Experimental constraints on the partitioning of Cl between topaz rhyolite melt and H_2O and $H_2O + CO_2$ fluids: new implications for granitic differentiation and ore deposition. Geochim. Cosmochim. Acta 52, 2091–2105.
Webster, J.D., Holloway, J.R., Hervig, R.L., 1989. Partitioning of lithophile trace elements between H_2O and $H_2O + CO_2$ fluids and topaz rhyolite melt. Econ. Geol. 84, 116–134.
Welin, E., 1966a. Uranium mineralizations and age relationships in the Precambrian bedrock of central and southeastern Sweden. Geol. Fören. Stock. Förh. 88, 34–67.
Welin, E., 1966b. Two occurrences of uranium in Sweden – the Los cobalt deposit and the iron ores of the Västervik area. Geol. Fören. Stock. Förh. 87, 492–508.
Weng, Z., Jowitt, S.M., Mudd, G.M., Haque, N., 2015. A detailed assessment of global rare earth element resources: opportunities and challenges. Econ. Geol. 110, 1925–1952.
Westra, L., Elbers, F.J., Sijperda, W.S., 1969. Investigations in the Västervik area, Southeastern Sweden: 1. Structural geology and genesis of the "younger" granites. Geol. Mijnbouw. 48, 529–544.
Williams-Jones, A.E., Migdisov, A.A., 2014. Experimental constraints on the transport and deposition of metals in ore-forming hydrothermal systems. Econ. Geol. Special pub. 18, 77–95.
Williams-Jones, A.E., Migdisov, A.A., and Samson, I.M., 2012. Hydrothermal mobilisation of the rare earth elements – a tale of "ceria" and "yttria". Elements, 8, 355–360.
Williams-Jones, A.E., Wollenberg, R., Bodeving, S., 2015. Hydrothermal fractionation of the rare earth elements and the genesis of the Lofdal REE deposit, Namibia. In: Simandl, G.J, Neetz, M., (Eds.), Symposium on strategic and critical materials proceedings, November 13-14, 2015, Victoria, British Columbia, British Columbia Ministry of Energy and Mines, British Columbia Geological Survey Paper 2015-3, 125–130.
Wolf, M.B., London, D., 1994. Apatite dissolution into peraluminous haplogranitic melts: an experimental study of solubilities and mechanisms. Geochim. Cosmochim. Acta 58, 4127–4145.
Wolf, M.B., London, D., 1995. Incongruent dissolution of REE- and Sr-rich apatite in peraluminous granitic liquids: differential apatite, monazite, and xenotime solubilities during anatexis. Am. Mineral. 80, 765–775.
Wood, S.A., 1990. The aqueous geochemistry of the Rare-Earth Elements and Yttrium 2. Theoretical predictions of speciation in hydrothermal solutions to 350 °C at saturation water vapor pressure. Chem. Geol. 88, 99–125.
Wood, S., Palmer, D., Wesolowski, D., Bénézeth, P., 2002. The aqueous geochemistry of the rare earth elements and yttrium. Part XI. The solubility of $Nd(OH)_3$ and hydrolysis of Nd^{3+} from 30 to 290 °C at saturated water vapor pressure with in-situ pHm measurement. In: Hellmann, R., Wood, S.A. (Eds.), Water-rock interactions, ore deposits, and environmental geochemistry: a tribute to David A. Crerar, pp. 229–256.
Woodard, J., Hetherington, C.J., 2014. Carbonatite in a post-collisional tectonic setting: geochronology and emplacement conditions at Naantali, SW Finland. Precambrian Res. 240, 94–107.
Xing, Y., Etschmann, B., Liu, W., Mei, Y., Shvarov, Y., Testemale, D., Tomkins, A., Brugger, J., 2019. The role of fluorine in hydrothermal mobilization and transportation of Fe, U and REE and the formation of IOCG deposits. Chem. Geol. 504, 158–176.
Xu, C., Campbell, I.H., Kynicky, J., Allen, C.M., Chen, Y., Huang, Z., Qi, L., 2008. Comparison of the Daluxiang and Maoniuping carbonatitic REE deposits with Bayan Obo REE deposit, China. Lithos 106, 12–24.
Zaitsev, A.N., Terry Williams, C., Jeffries, T.E., Strekopytov, S., Moutte, J., Ivashchenkova, O. V., Spratt, J., Petrov, S. V., Wall, F., Seltmann, R., Borozdin, A.P., 2015. Rare earth elements in phoscorites and carbonatites of the Devonian Kola Alkaline Province, Russia: examples from Kovdor, Khibina, Vuoriyarvi and Turiy Mys complexes." Ore Geol. Rev. 64, 477–498.
Zajacz, Z., Halter, W.E., Pettke, T., Guillong, M., 2008. Determination of fluid/melt partition coefficients by LA-ICPMS analysis of co-existing fluid and silicate melt inclusions: controls on element partitioning. Geochim. Cosmochim. Acta 72, 2169–2197.
Zhu, C., Sverjensky, D.A., 1991. Partitioning of F-Cl-OH between minerals and hydrothermal fluids. Geochim. Cosmochim. Acta 55, 1837–1858

Appendix

Table A1. Summary of microthermometric data of measured fluid inclusions.

Sample	FI Assemblage	Type	Tm Ice	Tm Halite	Tm Ant[1]	Th (Min)	Th (Max)	Th	Th mode	Tm CO_2	Th CO_2	Th CO_2 mode	Salinity (wt%)
OLR12001-26.5	FIA1	L-V-S, Na-Fe-K-Ca brine		290		120	280*	170	L-V-S → L-S				45.0
OLR12001-26.5	FIA11	L-V-S, Na-Fe-K-Ca brine		309		207	279*	219	L-V-S → L-S				45.0
OLR12001-26.5	FIA21	L-V-S, Na-Fe-K-Ca brine		304		115	227	162	L-V-S → L-S				45.0
OLR12001-26.5	FIA5	L-V-S, Na-Fe-K-Ca brine		304		130	304*	190	L-V-S → L-S				45.0
OLR12001-26.5	FIA9	L-V-S, Na-Fe-K-Ca brine		310		186	234	206	L-V-S → L-S				45.0
OLR12001-26.5 #2	FIA24	L-V-S, Na-Ca brine	–27.8	143		130	155	138	L-V-S → L-S				31.3
OLR12001-26.5 #2	FIA25	L-V-S, Na-Ca brine	–26.6	130		90	137	105	L-V-S → L-S				30.6
DJU18	FIA2	L-V-S, Ca-Na brine		150		145	176*	165	L-V-S → L-S				47.9 (0.13) #
DJU18	FIA23	L-V-S, Ca-Na brine		119		144	307*	283	L-V-S → L-S				46.6 (0.08) #
DJU18	FIA29	L-V-S, Ca-Na brine		137		84	104	89	L-V-S → L-S				46.1
DJU18	FIA8	L-V-S, Ca-Na brine		148		60	128	98	L-V-S → L-S				47.9
EJ-14-2A	FIA12	L-V-S, Ca-Na brine		173		91	117	104	L-V-S → L-S				52.0 (0.13) #
EJ-14-2A	FIA23	L-V-S, Ca-Na brine		126		84	159*	104	L-V-S → L-S				44.7 (0.12) #
EJ-14-2A	FIA9	L-V-S, Ca-Na brine		177		108	143*	131	L-V-S → L-S				49.6 (0.17) #
EJ-14-2B	FIA22	L-V-S, Ca-Na brine		187		105	162	145	L-V-S → L-S				55.5 (0.12) #
EJ-14-2B	FIA9	L-V-S, Ca-Na brine		171		70	119	100	L-V-S → L-S				52.0
DJU18	FIA4	L-V, medium salinity	–5.9			n.m.	n.m.	n.m.					9.0
EJ-14-2A	FIA24	L-V, medium salinity	–4.5			237	408	306	L-V → L				7.1
OLR12001-26.5 #2	FIA11	L-V, medium salinity	–9.5			94	105	101	L-V → L				13.4
OLR12001-26.5 #2	FIA12	L-V, medium salinity	–16.2			95	104	95	L-V → L				19.6
DJU09	FIA20	L-V, low salinity, heterogeneously trapped	–0.2			239	374	331	L-V → L				0.4
DJU18	FIA10	L-V, low salinity, heterogeneously trapped	–0.3			251	399	333	L-V → L				0.5
DJU26	FIA15	L-V, low salinity, heterogeneously trapped	–0.3			279	375	356	L-V → L				0.4

Table A1 continuation

Sample	FI Assemblage	Type	Tm Ice	Tm Halite	Tm Ant[1]	Th (Min)	Th (Max)	Th	Th mode	Tm CO_2	Th CO_2	Th CO_2 mode	Salinity (wt%)
DJU26	FIA17	L-V, low salinity, heterogeneously trapped	–0.4			315	367	357	L-V → L				0.7
EJ-14-2A	FIA30	L-V, low salinity	–0.6			236	327	248	L-V → L				0.9
OLR12001-26.5	FIA10	Co-existing L-V-S Na-Fe-K-Ca brine and CO_2		290		120	295*	245	L-V-S → L-S	–56.1	29.6	L_{CO2}-V_{CO2}-(L_{H2O}) → L_{CO2}-(L_{H2O})	40.0
DJU09	FIA18	Co-existing L-V-S Ca-Na brine and CO_2		180		107	107	107	L-V-S → L-S	–57	27	L_{CO2}-V_{CO2}-(L_{H2O}) → L_{CO2}-(L_{H2O})	53.7
EJ-14-2B	FIA17	Co-existing L-V-S Ca-Na brine and CO_2		175	24.8	120	130	120	L-V-S → L-S	–56.8	n.m.		49.3
EJ-14-2A	FIA15	Co-existing CO_2 and L-V with varying salinity	–15.9			n.m.	n.m.	n.m.		–56.9	27.3	L_{CO2}-V_{CO2}-(L_{H2O}) → L_{CO2}-(L_{H2O})	19.3
EJ-14-2B	FIA19	Co-existing CO_2 and L-V with varying salinity	–21.9			n.m.	n.m.	n.m.					23.6
EJ-14-2A	FIA25	CO_2								–56.9	12.1	L_{CO2}-V_{CO2}-(L_{H2O}) → L_{CO2}-(L_{H2O})	
EJ-14-2A	FIA29	CO_2								–56.7	27	L_{CO2}-V_{CO2}-(L_{H2O}) → L_{CO2}-(L_{H2O})	
OLR12001-26.5 #2	FIA16	CO_2								–56	30.4	L_{CO2}-V_{CO2}-(L_{H2O}) → L_{CO2}-(L_{H2O})	
OLR12001-26.5 #2	FIA19	CO_2								–55.9	30.6	L_{CO2}-V_{CO2}-(L_{H2O}) → L_{CO2}-(L_{H2O})	

Data for the assemblages are reported as the median of several inclusions except for the minimum and maximum Th values; n.m. = not measured.

[1] Melting of antarcticite ($CaCl_2 \cdot 6H_2O$) verified by Raman spectroscopy.

* Th and Tm (halite) measured after LA-ICP-MS analysis; high homogenisation temperatures may indicate stretching of fluid inclusions during ablation.

Value in the bracket is the measured Na/(Na+Ca) mass ratio from LA-ICP-MS analysis.

Table A2.. Summary of fluid inclusion LA-ICP-MS data. Data reported as averages of fluid inclusions assemblages.

Sample	OLR12001-26.5	OLR12001-26.5 #2	OLR12001-26.5 #2	OLR12001-26.5 #2	OLR12001-26.5 #2	OLR12001-26.5 #2	EJ-14-2A	DJU18	EJ-14-2B	DJU18	EJ-14-2A	EJ-14-2A	OLR12001-26.5 #2	OLR12001-26.5 #2
FI Assemblage	FIA1	FIA13	FIA20	FIA6	FIA24	FIA25	FIA12	FIA2	FIA22	FIA23	FIA23	FIA9	FIA11	FIA12
Type	L-V-S, Na-Fe-K-Ca brine	L-V-S, Na-Fe-K-Ca brine	L-V-S, Na-Fe-K-Ca brine	L-V-S, Na-Fe-K-Ca brine	L-V-S, Na-Ca brine	L-V-S, Na-Ca brine	L-V-S, Ca-Na brine	L-V-S, Ca-Na brine	L-V-S, Ca-Na brine	L-V-S, Ca-Na brine	L-V-S, Ca-Na brine	L-V-S, Ca-Na brine	L-V, medium salinity	L-V, medium salinity
Salinity (wt%)	45.0	45.0	45.0	45.0	31.0	30.5	52.0	48.0	55.5	46.5	45.0	50.0	13.5	19.5
NaCl	29.0	22.6	24.6	23.7	17.2	18.6	6.2	5.9	6.0	3.5	5.0	7.8	11.8	9.8
$CaCl_2$	7.0	5.7	4.4	7.5	11.3	9.4	45.8	42.1	49.5	43.0	40.0	42.2		3.2
KCl	9.0	6.3	7.0	5.8	2.5	2.5							1.7	6.5
$FeCl_2$		10.4	9.0	8.0										
Li (ppm)	42.9	67	85.4	38.4	33.1	51.4	24.5	63.5	32.8	118	18.1	24.6	98.8	55.3
B	183	261	1810	209	102	276	919	391	<14	418	98	255	<1	271
Na	114000	88818	96640	93325	67583	73075	24402	23352	23450	13814	19543	30718	46400	38650
Mg	n.a.	116	76.8	50.4	554	1386	688	724	960	<0.04	115	157	116	269
Al	n.a.	n.a.	n.a.	n.a.	n.a.	n.a.	n.a.	*14430*	n.a.	<0.4	*2865*	*5840*	n.a.	n.a.
K	47067	33109	36660	30238	13183	13351	3278	2270	1768	1141	1034	2473	8950	34100
Ca	25433	20709	15920	27181	40850	33863	165462	151857	178800	155143	144625	152500	2470	11460
Ti	<0.1	n.a.	n.a.	n.a.	n.a.	n.a.	n.a.	<0.6	n.a.	<0.2	*10*	<0.5	n.a.	n.a.
Mn	7263	5716	3680	5465	889	611	58	198	412	70.7	17.2	<0.2	<1.2	183
Fe	n.a.	45736	39700	35250	n.a.	3490	*10232*	*4703*	n.a.	<8	*922*	*1223*	1370	4508
Zn	4073	3396	946	3631	11113	15088	102	87.8	132	11	1.3	109	n.p.	2545
Rb	465	295	405	425	254	197	37.7	19.9	22.8	13.9	11.6	32.0	56.6	175
Sr	2130	1675	89.3	2046	6867	9764	214	494	668	467	336	192	253	705
Cs	185	95.9	145	135	240	133	9.2	1.2	18.1	1.2	3.7	8.7	4.7	40.5
Ba	1437	1072	77.2	1515	3498	3359	92.3	31.8	174	25.5	12.8	45.1	14.9	34.8

Table A2 continuation

Sample	OLR12001-26.5	OLR12001-26.5 #2	OLR12001-26.5 #2	OLR12001-26.5 #2	OLR12001-26.5 #2	OLR12001-26.5 #2	EJ-14-2A	DJU18	EJ-14-2B	DJU18	EJ-14-2A	EJ-14-2A	OLR12001-26.5 #2	OLR12001-26.5 #2
FI Assemblage	FIA1	FIA13	FIA20	FIA6	FIA24	FIA25	FIA12	FIA2	FIA22	FIA23	FIA23	FIA9	FIA11	FIA12
Type	L-V-S, Na-Fe-K-Ca brine	L-V-S, Na-Fe-K-Ca brine	L-V-S, Na-Fe-K-Ca brine	L-V-S, Na-Fe-K-Ca brine	L-V-S, Na-Ca brine	L-V-S, Na-Ca brine	L-V-S, Ca-Na brine	L-V-S, Ca-Na brine	L-V-S, Ca-Na brine	L-V-S, Ca-Na brine	L-V-S, Ca-Na brine	L-V-S, Ca-Na brine	L-V, medium salinity	L-V, medium salinity
Pb (ppm)	2233	1595	376	1732	5105	6336	605	20.2	1827	92.3	15.3	443	<0.07	938
P	n.a.	<3	<59	<30	<9.5	<13	<3	<19	<70	<4	n.a.	n.a.	<5	<8
Y	<0.01	<0.03	<0.2	0.87	<0.02	<0.03	3.59	1.49	1.03	1.42	n.a.	n.a.	<0.01	<0.03
Ce	0.85	1.24	<0.3	0.95	<0.01	<0.02	7.7	33.95	8.54	10.3	n.a.	n.a.	<0.01	<0.03
Nd	<0.02	<0.1	<1.2	<0.3	<0.07	<0.3	0.17	16.5	1.74	8.82	n.a.	n.a.	<0.04	<0.1
Cl	356333	265000	201000	257188	191333	190875	209923	266619	273000	214714	250250	230000	81950	68875
Br	1910	744	880	1056	1974	4486	3183	6195	11182	2053	972	3047	n.p.	25
I	18.4	10.5	16.5	14.8	45.6	50	68.4	95.7	332	54.3	13.2	80.5	n.p.	<0.8
Br/Cl · 10^{-3} (molar)	2.4	1.2	1.9	1.8	4.6	10.4	6.7	10.3	18.2	4.2	1.7	5.9		0.2
I/Cl · 10^{-6} (molar)	14	11	23	16	67	73	91	100	339	71	15	98		

n.a. = not analysed during LA-ICP-MS analytical session.

n.p. = not present in fluid inclusion, the element was removed during data processing.

Values in *italic* (for Al, Fe, and Ti) are uncertain and erratic; high concentrations may have resulted from analysed trapped solid inclusions in the fluid inclusions.